Details of the research work duly signed by the applicant (Dr. Sanyog Jain), for which the Sun Pharma Research Award is claimed

Project title: Combination drug therapy using nanotechnology for cancer therapeutics

Introduction

Cancer remains a formidable global health challenge, characterized by its high incidence and mortality rates. The therapy of cancer involves use of neo-adjuvant chemotherapy, surgery, and radiotherapy. The limitations and disappointing clinical outcomes associated with conventional cancer therapies are often attributed to the development of resistance and significant toxicity toward healthy tissues. Recent progress in cancer treatment has transitioned from emphasizing monotherapy to prioritizing combined treatments, capitalizing on collaborative enhancements between diverse therapies to potentially yield remarkably amplified therapeutic outcomes and achieve optimal synergy. Advancements in our understanding of tumor biology, molecular pathways, the tumor microenvironment, and tumor-host interactions have paved the way for innovative combination therapies. These include a combination of chemotherapy with immunotherapy, targeted therapy, gene therapy (including DNA and RNA-based approaches), and epigenetic therapy. This approach potentially reduces drug resistance, while simultaneously providing therapeutic anti-cancer benefits, such as reducing tumour growth and metastatic potential, arresting mitotically active cells, reducing cancer stem cell populations, and inducing apoptosis. This multi-agent therapy can modulate different signaling pathways, thereby hitting different targets which can improve the therapeutic index either in the form of better efficacy or reduced toxicity. However, due to the degradation of drugs before being delivered to a target site, the difference between the ratio of the two therapeutics at the site of action and the initially designed ratio poses a significant challenge in delivery. Additionally, unifying the pharmacokinetics of the individual drugs, on-target accumulation, and intracellular uptake of various drug molecules are major concerns that need to be addressed to get control over dosage for maximal therapeutic efficacy. Despite achieving significant advancement in the co-delivery of drugs and/or genes, these issues need to be solved before engaging in clinical application.

Dual drug therapies, like drug-drug conjugates and nanoparticle-drug conjugates may help to overcome non-specific target action and toxicity by selectively targeting to tumour cells and consequently acting at multiple drug targets, thereby achieving therapeutic synergy. These approaches increase versatility by either creating a novel pharmacophore or by enhancing the potency of a drug. Drug conjugates can be directly linked or are connected by cleavable or non-cleavable spacer molecules like PEG to exert synergistic action at biological targets. Conjugation of two different agent to single linker allows same body distribution and prolongs circulation time, hence, maximizing benefit of the combination. Moreover, this strategy can also be used in cases where the structural arrangement of molecules significantly contributes to the induction of toxicity. Conjugation of such compounds with another therapeutic element can render the molecule safe for administration. On the other hand,

nanoformulation has proved to be a great strategy for incorporating two different drugs within the same vicinity, which would further exert their effects in a controlled manner and most importantly reduce in frequency of administration. The controlled release functionality provided by the nanoparticle system can standardize the pharmacokinetics, biodistribution, and stability of the drug. The drug that may exhibit highly diverse chemical properties can be loaded into nanoformulation which would have otherwise resulted in distinct pharmacological responses. Apart from exhibiting synergism by utilizing different class of drug modulating the pathways, reversal of chemoresistance can also be achieved by delivering therapeutics with chemosensitizer elements. These approaches form a bridge between therapeutics and biomaterial which can be a promising strategy for clinical application. My research group is extensively worked on combination therapy for treatment of cancer. Below is the brief description of the work we implemented by my group:

- **Brief research report 1**

Dual acting Cisplatin (IV) Prodrugs for Safer Synergistic Chemotherapy

Cisplatin is a 1st-generation platinum drug that induces multifaceted cell death via DNA cross-linking, inhibiting transcription, replication, and triggering ROS-mediated pathways like ferroptosis. However, the clinical applicability of cisplatin is constrained by limited by resistance, dose-dependent toxicity (e.g., nephrotoxicity), and off-target interactions. Further, the inherent structural attributes confer high kinetic reactivity and hydrophilicity causing off-target interaction that engenders substantial toxicity and impedes cellular internalization. The overall challenges undermine the therapeutic potential and increase the risk-to-benefit ratio for cisplatin therapy. Designing synergistic dual-acting Pt (IV) prodrugs with central Pt atoms and axial ligands is a potent approach to overcome challenges. Based on the type of axial ligand the biophysical properties of the parent molecule could be tailored. These prodrugs possess stable d6 electronic configuration and undergo bioconversion to the parent drug in a reducing environment through electron-reductive elimination.

We have designed safer cisplatin (IV) prodrugs with diverse bioactive ligands—valproate (VA), tocopherol succinate (TOS), and chlorambucil (CBL). These prodrugs exhibit synergistic dual action by targeting multiple pathways in triple-negative breast cancer. They adopt octahedral geometry, increasing stability during ligand substitution and reducing drug deactivation in transit to tumor cells. Strategic axial ligand placement enhances antitumor efficacy, customizes lipophilicity, and improves cellular uptake. The prodrugs' d6 electronic configuration ensures stability under physiological conditions, while they release the parent drug and axial ligands through reduction in the tumor microenvironment. The dual-acting cisplatin (IV) prodrugs were synthesized, using three bioactive ligands (VA, TOS, CBL) at a 1:2 cisplatin: axial ligand ratio (CP-VA, CP-TOS, CP-CBL). After synthesis, all conjugates underwent dialysis to eliminate solvent traces, followed by lyophilization. We first assessed the influence of axial ligands on the biophysical characteristics of cisplatin, e.g., kinetic stability followed by anti-tumor efficacy studies. The cisplatin (IV) prodrugs displayed notable log P values: CP-VA (~0.28), CP-TOS (~1.39), and CP-CBL (~1.75), than cisplatin (~ -2.27) thus enhancing lipophilicity-related biopharmaceutical aspects such as cellular

uptake. The designed prodrugs exhibited excellent stability and minimal drug content loss in both PBS (<10%) and BSA (<15%) over 12 hours. In contrast, the free drug experienced over 90% drug content loss within just 2 hours of incubation. This trend was also reflected in the CD spectrum, where prodrugs had no significant impact on BSA structure compared to the evident spectral shift seen with the free drug. Prodrugs exhibited rapid reduction of Pt (IV) content (>55% in 2h) in reducing media (GSH and ascorbate) with short reduction $t_{1/2}$ (<3.68h) while remaining stable in PBS (<90% reduction, $t_{1/2}$ >12h) till 12h. Notably, enhanced total Pt uptake was observed with a dose-dependent reduction in cell viability in MDA-MB-231 and A549 cell lines. In presence of copper transporter inhibitor (Ctr1) cisplatin demonstrated reduced Pt uptake in (~3.2-fold) MDA-MB-231 and (~2.3-fold) A549 cell lines while Pt (IV) prodrugs CP-VA (~10.64-fold, ~11.44-fold), CP-CBL (~17.66-fold, ~22.51-fold), and CP-TOS (~26.87-fold, ~31.77-fold) exhibited significant uptake in MDA-MB-231 and A549 cell lines. These results indicated the effectiveness of the Pt (IV) prodrug approach in improving cellular drug uptake and minimizing the transporter-dependent drug uptake. In MDA-MB-231 and A549 cells drug lipophilicity was found to directly influence the amount of drug internalized with R^2 values of 0.9844 and 0.9874, respectively. Simulation studies revealed drug (cisplatin polygon)-encapsulating characteristic of CP-TOS whereas CP-CBL and CP-VA prodrugs showed open structure. Out of three Pt (IV) derivatives, CP-TOS exhibited good self-assembling potential in a nano-meter range which could assist in passive tumor targeting. An insignificant change in RBC morphology was observed indicating the biocompatibility of Pt (IV) prodrugs. Remarkable intra-tumoral Pt accumulation was observed which could be due to improved lipophilicity and reduced drug loss. Developed prodrugs showed synergistic action (CI <1) with significant dose reduction of cisplatin (~2-5-fold) as compared to physical mixtures in all cell lines (A549, SKOV-3, MCF-7, MDA-MB-231, HeLa, and U87). The developed cisplatin (IV) prodrugs exhibited superior anti-proliferative action with a notable reduction in IC_{50}. These effects were more pronounced in the MDA-MB-231 cell line proving the sensitivity of TNBC towards Pt therapy. Sulphorhodamine B assay in the MDA-MB-231 cell line showed a similar outcome. In contrast to the free drug, CP-VA, CP-CBL, and CP-TOS treatments showed significant Pt uptake (5.1, 7.1, and 9.9-fold, respectively). In the presence of copper transporter inhibitor, the prodrugs displayed a minimal reduction in Pt uptake compared to cisplatin (2-3-fold decrease). Cisplatin (IV) prodrugs substantial depletion in GSH levels coupled with increased ROS levels, triggering apoptosis. This was corroborated by an apoptosis assay, which demonstrated a transition toward early and late apoptotic stages. Moreover, there was a decrease in the G_0-G_1 cell population, concomitant with an increase in the S phase, indicative of an enhanced DNA damaging potential. All three cisplatin (IV) prodrugs demonstrated mitochondrial membrane depolarization with increased levels of cellular ions (K^+, Ca^{2+}) indicating apoptosis induction. Further, demonstrated high DNA damaging intensity with increased caspase-3 level denoting improved apoptosis potential. *In vivo,* studies employing CP-VA, CP-TOS, and CP-CBL revealed superior reductions in tumor volume (~1.9, ~3.4, and ~7.2) and tumor weight (~1.5, ~2.8, and ~6.1) compared to cisplatin. Minimal elevation in liver (ALT, AST, and ALP) and kidney (BUN and creatinine) biomarkers was observed, implying an enhanced safety profile for cisplatin (IV) prodrugs.

Highlighted experimental outcomes:

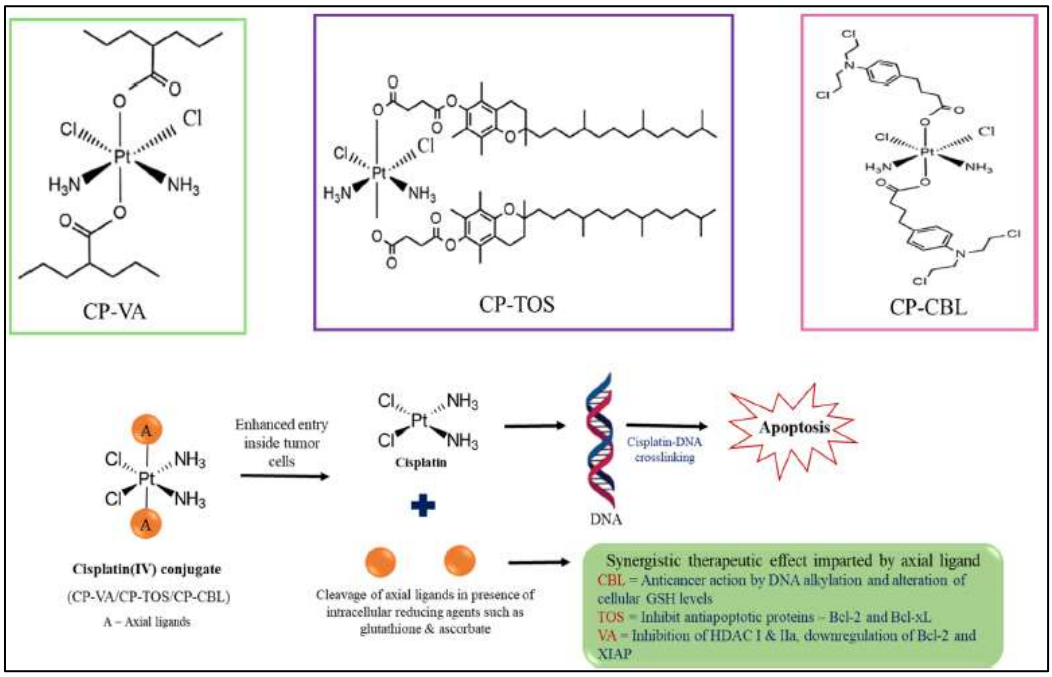

Figure 1: Graphical illustration of the chemical structure of developed cisplatin (IV) conjugates their mechanism of intracellular reduction, and their subcellular targets for synergistic therapeutic action

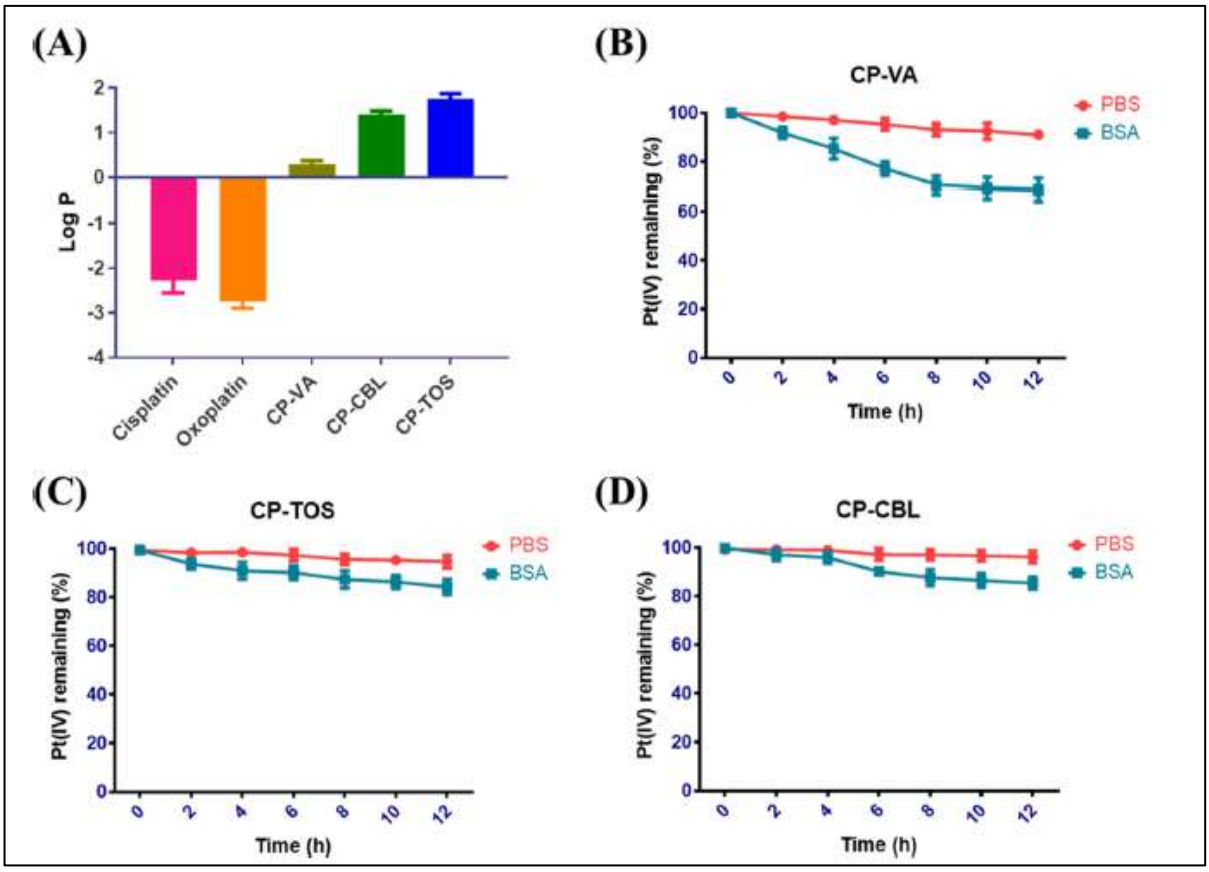

Figure 2: illustrates A) Partition coefficient (log P) of cisplatin and cisplatin (IV) derivatives in the octanol: water system B) Stability kinetics of CP-VA, C) CP-TOS, and D) CP-CBL in PBS (pH 7.4) and BSA solution for 12 h incubation at 37 °C.

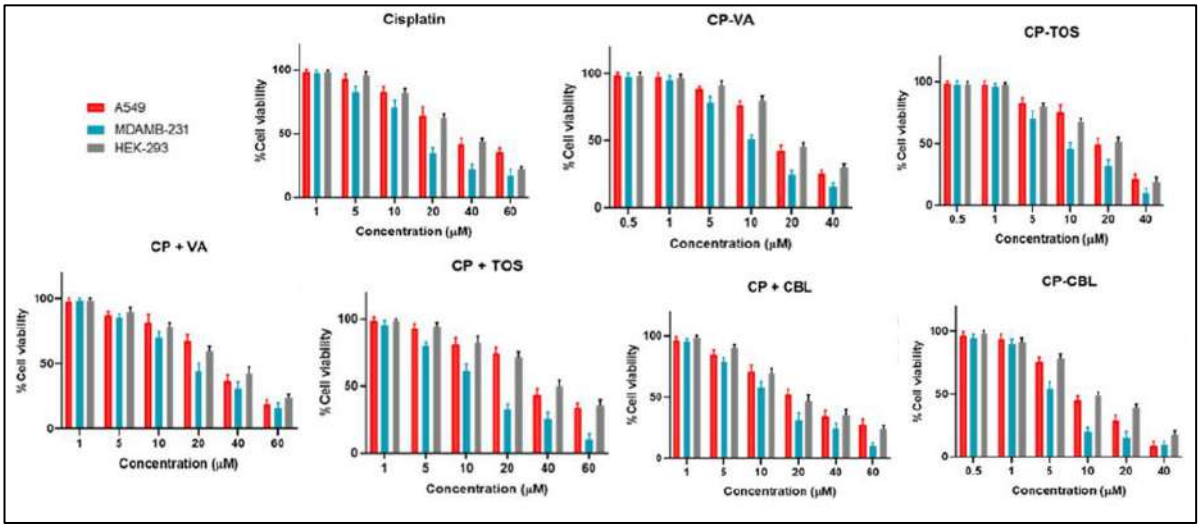

Figure 3: represents Cell viability versus drug concentration plots after treatment of A549, MDA-MB-231, and HEK-293 cells with cisplatin, cisplatin (IV) derivatives, and physical mixture for 24 h

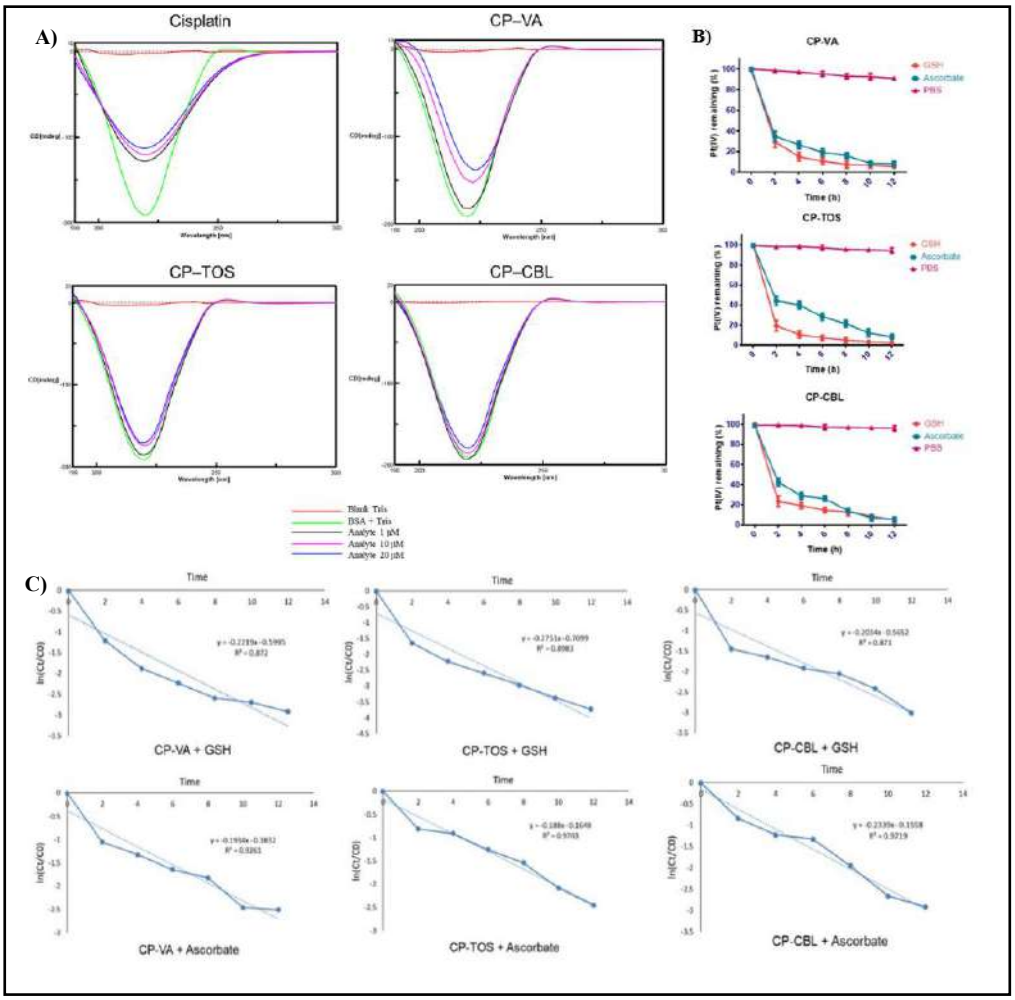

Figure 4: illustrates A) Circular dichroism spectroscopic analysis of (I) cisplatin, (II) CP-VA, (III) CP-TOS (IV) CP-CBL, after 24 h incubation of BSA B) Reduction profiles of cisplatin (IV) prodrugs in reducing media (GSH & ascorbate) and PBS solution for 12 h incubation at 37 °C. C) ln(Ct/C0) versus time plot for reduction kinetic analysis of designed cisplatin(IV) derivatives in GSH and ascorbate solution at 37 °C

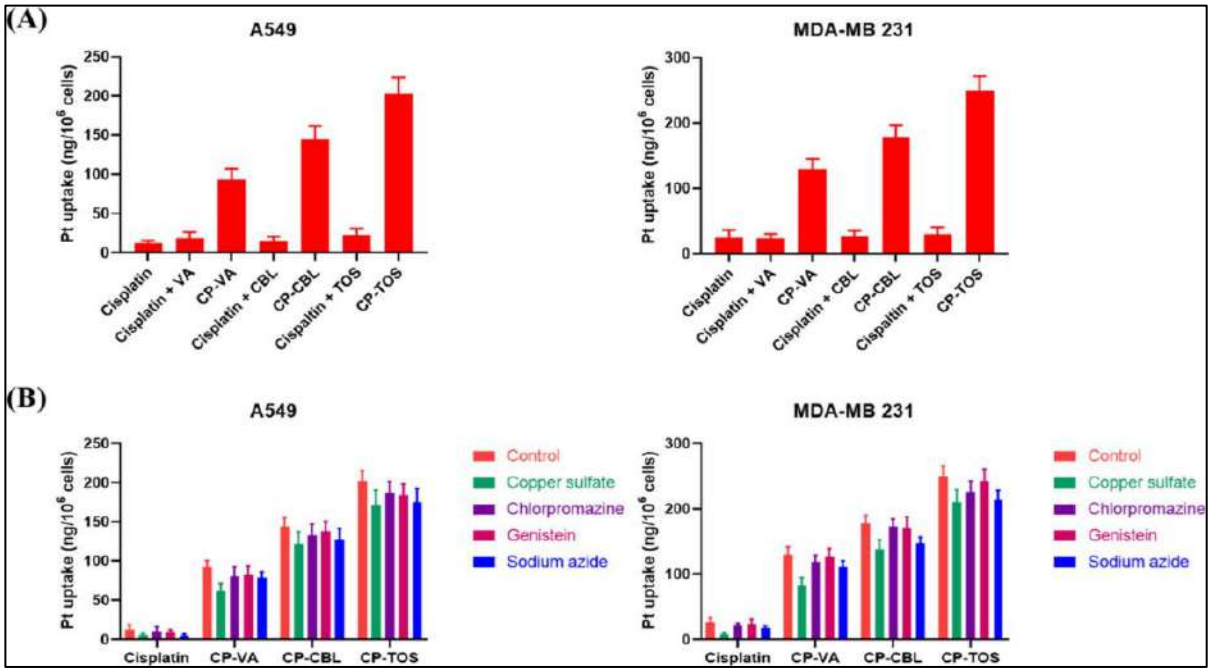

Figure 5: illustrates A) Cellular platinum levels and B) Pt levels in presence of uptake inhibitors after exposing A549 and MDA-MB-231 cells cisplatin, cisplatin + axial ligand physical mixture (1:2 mole ratio), and cisplatin (IV) conjugates for 24 h

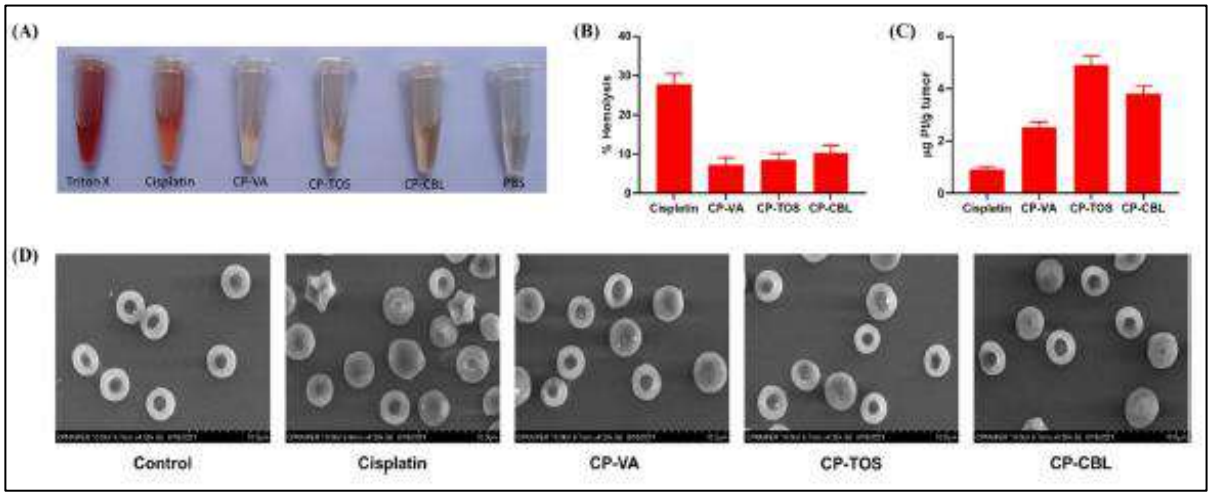

Figure 6: highlights (A) a representative image of RBC suspension exposed to different treatment groups (B) % hemolysis observed in RBCs (C) amount of platinum detected in tumors excised from animals (10 mg/kg Pt equivalent dose) (n = 3) (D) SEM images of RBC samples exposed to 20 µg/mL of each test compound along with PBS as a control

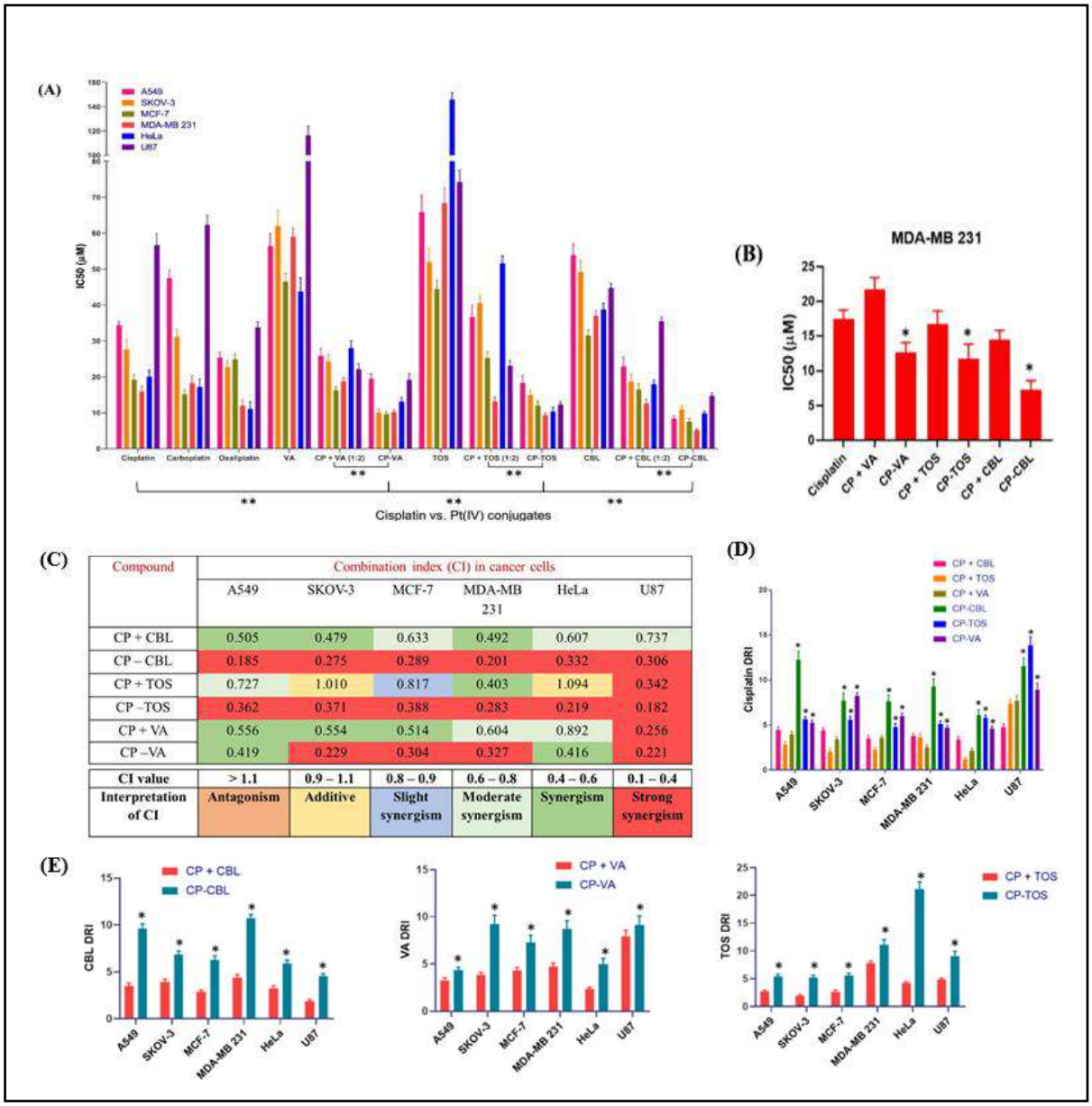

Compound	Combination index (CI) in cancer cells					
	A549	SKOV-3	MCF-7	MDA-MB 231	HeLa	U87
CP + CBL	0.505	0.479	0.633	0.492	0.607	0.737
CP – CBL	0.185	0.275	0.289	0.201	0.332	0.306
CP + TOS	0.727	1.010	0.817	0.403	1.094	0.342
CP –TOS	0.362	0.371	0.388	0.283	0.219	0.182
CP + VA	0.556	0.554	0.514	0.604	0.892	0.256
CP –VA	0.419	0.229	0.304	0.327	0.416	0.221
CI value	**> 1.1**	**0.9 – 1.1**	**0.8 – 0.9**	**0.6 – 0.8**	**0.4 – 0.6**	**0.1 – 0.4**
Interpretation of CI	**Antagonism**	**Additive**	**Slight synergism**	**Moderate synergism**	**Synergism**	**Strong synergism**

Figure 7: represents A) IC_{50} values obtained through MTT assay in various cell lines (**p < 0.0001) B) IC_{50} values obtained through sulphorhodamine B assay in MDA-MB 231 cells; (*p < 0.001) C) CI values in various cancer cell lines D) DRI values for cisplatin and E) DRI values for axial ligands in various cancer cell lines obtained after treatment; (*p < 0.05) for cisplatin(IV) derivatives compared with the respective physical mixture group

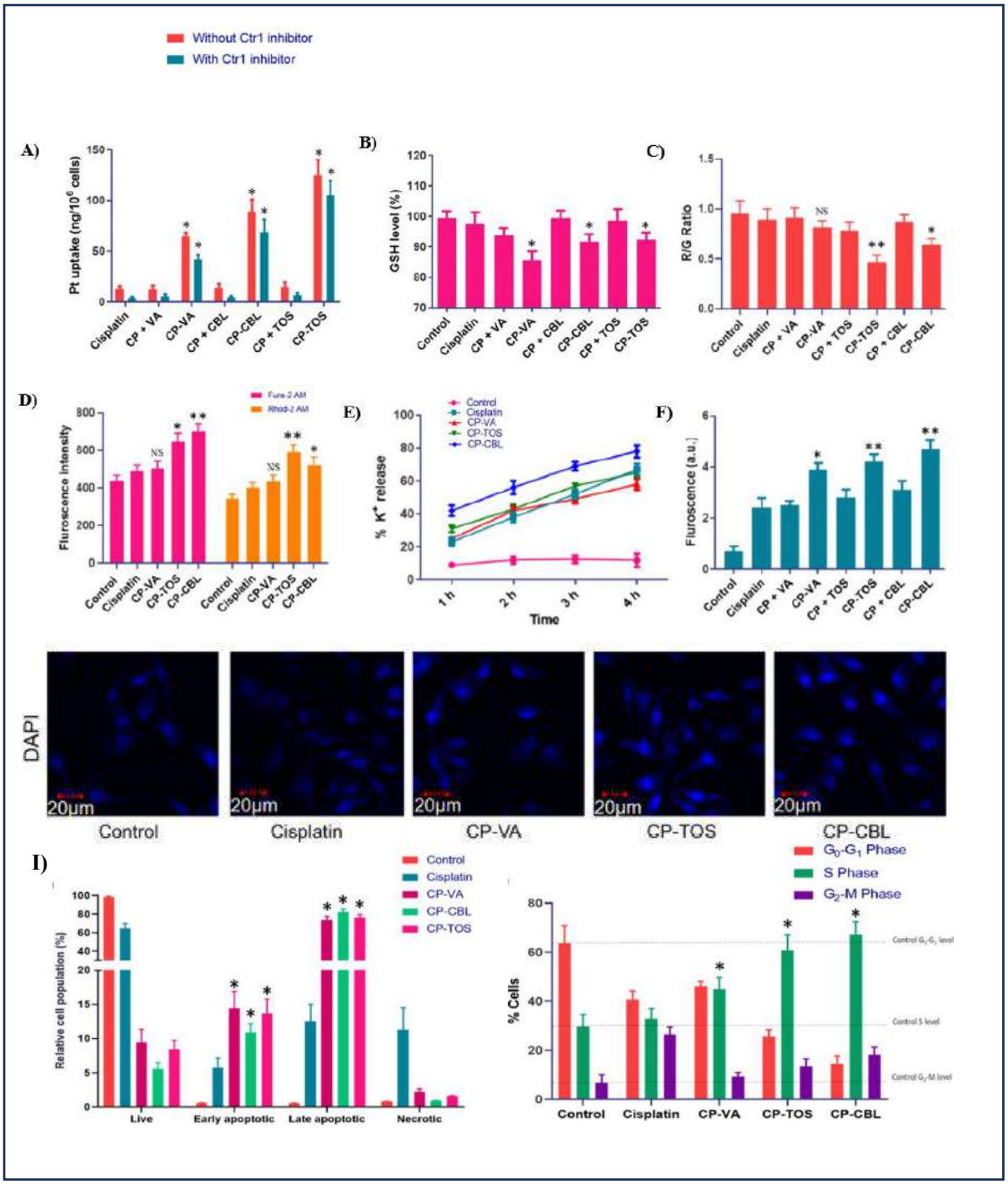

Figure 8: illustrates (A) Total Pt uptake in MDA-MB-231 cells in the presence and absence of Ctr1 inhibitor (*p < 0.0001) (B) Percent GSH level in MDA-MB- 231 cells after 24 h treatment with various test groups (*p < 0.01) (C) Mitochondrial membrane potential analysis by JC1 assay in MDA-MB-231 cells after treatment with test groups (*p < 0.01, **p < 0.0001, NS-statistically insignificant) (D-E) Percent of extracellular K+ ions released and cytosolic and mitochondrial Ca++ levels in MDA-MB-231 cells after drug treatment (*p < 0.001, **p < 0.0001) F) Caspase-3 levels in MDA-MB-231 cells after treatment with different test groups (*p < 0.001, **p < 0.0001) H) Intracellular ROS generation after treatment with test groups I) Flow cytometric analysis indicating apoptosis status J) Cell cycle pattern after treatment statistical significance (*p < 0.001) compared with cisplatin by two-way ANOVA

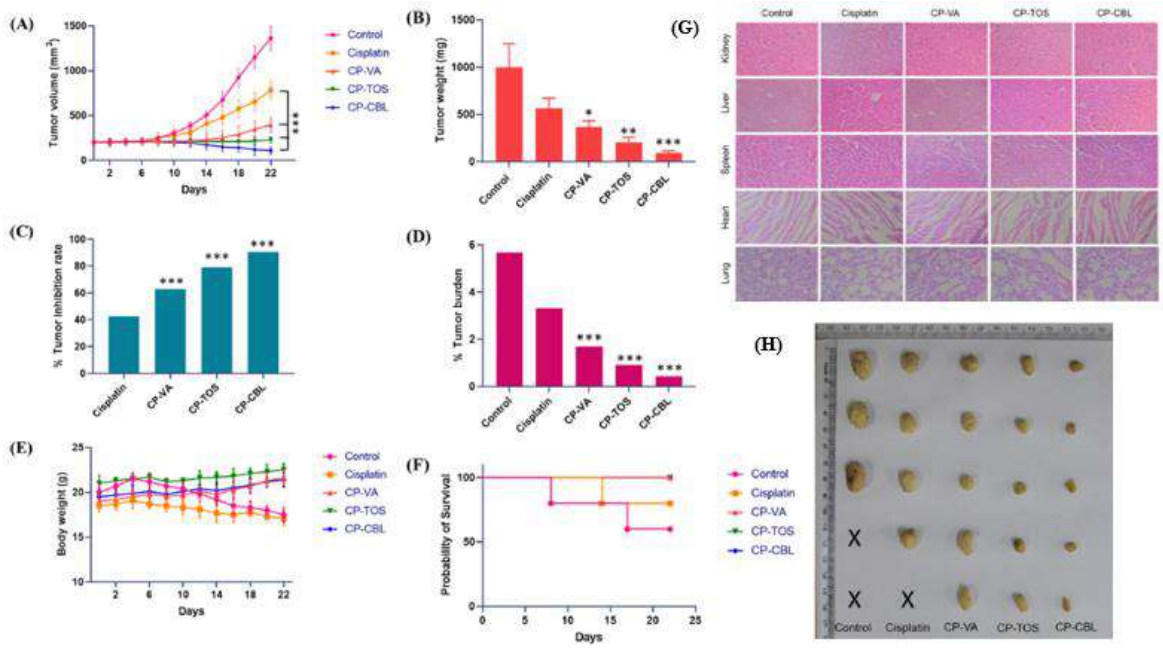

Figure 9: illustrates in vivo anticancer efficacy of cisplatin and designed cisplatin(IV) derivatives, (A) Tumor volume (B) Tumor weight (C) % tumor inhibition rate (D) % tumor burden (E) Change in body weight (F) Survival rate (G) histopathology analysis using H&E-stained images (H) Images of tumors excised from animals at the end of treatment (X-represent animal death before completion of study duration); (*$p < 0.05$, **$p < 0.001$, ***$p < 0.0001$) compared with cisplatin

Publications:

1. Tushar Date, Kaushik Kuche, Rohan Ghadi, Pradeep Kumar, **Sanyog Jain**, Understanding the role of axial ligands in modulating biopharmaceutical outcomes of cisplatin (IV) derivatives. **Molecular Pharmaceutics**, 19(5), 2022: 1325-1337 **(Impact factor: 4.9)**

2. Tushar Date, Kaushik Kuche, Dasharath Chaudhari, Rohan Ghadi, Deepak Kumar Sahel, Deepak Chitkara, **Sanyog Jain**, Hitting multiple cellular targets in triple-negative breast cancer using dual-action cisplatin (IV) prodrugs for safer synergistic chemotherapy. **ACS Biomaterials Science & Engineering**, 8(6), 2022: 2349-2362 **(Impact factor: 5.8)**

- **Brief research report 2**

Synergistic Combinatorial Therapeutic Strategy for Effective Cancer Treatment via Ferroptosis Induction

Ferroptosis is an oxygen-dependent, iron-catalyzed cell sabotage pathway that has gained significant attention as a form of cell death due to less complexity, no requirement for effector protein, direct control, and pro-immunogenic nature. This pathway is characterized by the accumulation of lipid reactive radicals that damage the plasma membrane's unsaturated fatty acids leading to ultimate cell destruction. However, the sensitivity of different cancer cells towards ferroptosis varies widely due to differences in metabolic, genetic, and signaling pathways. Considering these facts, combination therapy has emerged as a promising strategy. Combination therapy is a common approach to reduce toxicity, increase efficacy, and reduce chances of resistance. Thus, we conducted a comprehensive screening of novel synergistic drug combinations with Sorafenib (a cysteine/glutamate antiporter system inhibitor) to effectively induce ferroptosis-mediated cell death in different cancer cells. Additionally, we evaluated the *in vivo* anticancer activity and safety profile of the proposed synergistic combination therapy.

Different ferroptosis inducers were screened [simvastatin (SIM), phenethyl isothiocyanate (PITC), and trigonelline (TG)] for synergistic action sorafenib in three cell lines (MDA-MB-231, A549, and HeLa). A combination of SOR+SIM (1:1 w/w) exhibited higher cytotoxicity in MDA-MB-231 (3.97±0.59µg/mL), A549 (3.47±0.55 µg/mL), and HeLa (3.86±0.49 µg/mL). Meanwhile, SOR+PITC (MDA-MB-231, A549) and SOR+TG (A549) demonstrated notable cytotoxicity only in selective cell lines. In line with these results, the combination of SOR+SIM demonstrated a synergistic effect with CI<1 at all concentrations with favorable dose reduction at all Fa values. Based on synergy analysis, the synergistic combination of the SOR+SIM was established at all tested concentrations in the mentioned cancer cells. Intriguingly, in the presence of a ferroptosis inhibitor (Ferrostatin-1, 10µM) marked increase in cell viability was observed in MDA-MB-231 (~2.1-fold), A549 (~1.8-fold), and HeLa (~1.9-fold) indicating ferroptosis as a mechanism of cell death. Synergistic combination of SOR+SIM exhibited reduction in % GSH level, red/green fluorescence ratio, and increased MDA level proving ferroptosis induction. *In vivo* studies revealed SOR+SIM remarkable reduction in tumor volume as compared to the control (~3.53-fold), SIM(~2.55-fold), and SOR(~1.47-fold) monotherapies. Further combination of SOR+SIM was found to be biocompatible with an insignificant rise in biomarker level (ALT, AST, BUN, and Creatinine), with no signs of organ toxicity.

Highlighted experimental outcomes:

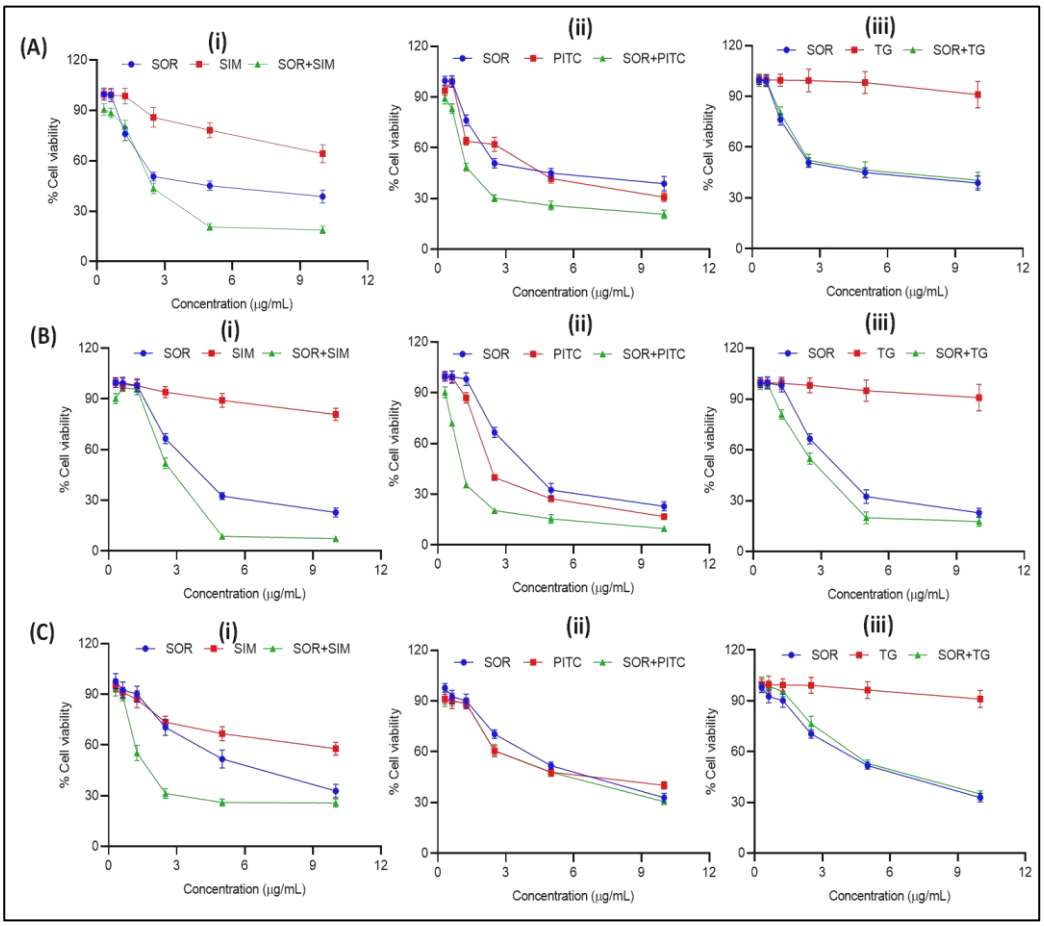

Figure 10: represents the % cell viability curve of monotherapy and in combination with SOR in (A) MDA-MB-231; (B) A549 and (C) HeLa cells.

Table 1. represents the combination index (CI) value of different combination with SOR in (A) MDA-MB-231; (B) A549 and (C) HeLa cells

Combinations	**Cells**		
	MDA-MB-231	**A549**	**HeLa**
SOR+SIM	0.660±0.041	0.536±0.099	0.592±0.040
SOR+PITC	0.741±0.046	0.576±0.015	1.699±0.103
SOR+TG	1.075±0.014	0.771±0.026	1.199±0.102
Colour codes	***Synergistic***	***Additive***	***Antagonistic***

Table 2. represents the dose reduction index (DRI) value of different combination with SOR in (A) MDA-MB-231; (B) A549 and (C) HeLa cells

Combinations	MDA-MB-231				A549				HeLa			
	SOR	SIM	PITC	TG	SOR	SIM	PITC	TG	SOR	SIM	PITC	TG
SOR+SIM	2.05±0.11	5.87±0.59	-	-	2.14±0.27	13.53±3.27	-	-	2.57±0.35	5.07±0.54	-	-
SOR+PITC	2.80±0.15	-	2.60±0.18	-	4.11±0.05	-	3.01±0.12	-	1.18±0.06	-	1.17±0.08	-
SOR+TG	0.96±0.02	-	-	39.64±0.44	1.39±0.04	-	-	17.82±1.45	0.87±0.07	-	-	22.87±1.15
Colour codes	***No dose reduction (~1)***				***Favourable dose reductions (≥2)***				***Un-favourable dose reduction (<1)***			

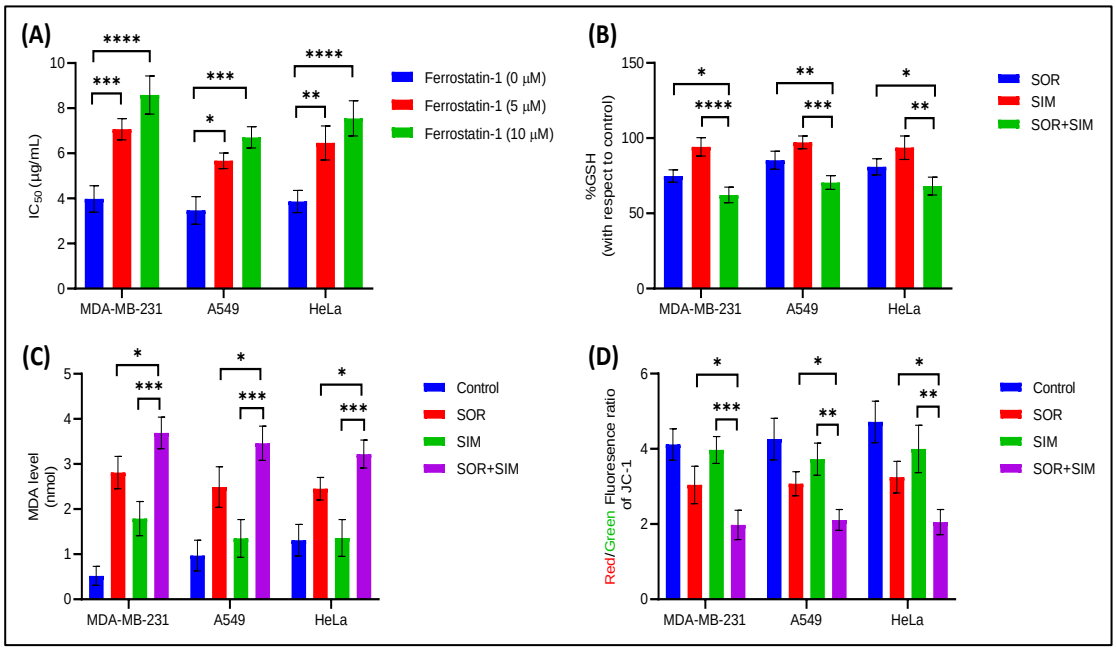

Figure 11: illustrates (A) % cell viability in presence of Ferrostatin-1 Panel (B-D) describes % GSH level, MDA level and MMP, herein *=P<0.05; **=P<0.01; ***=P<0.001 and ****=P<0.0001

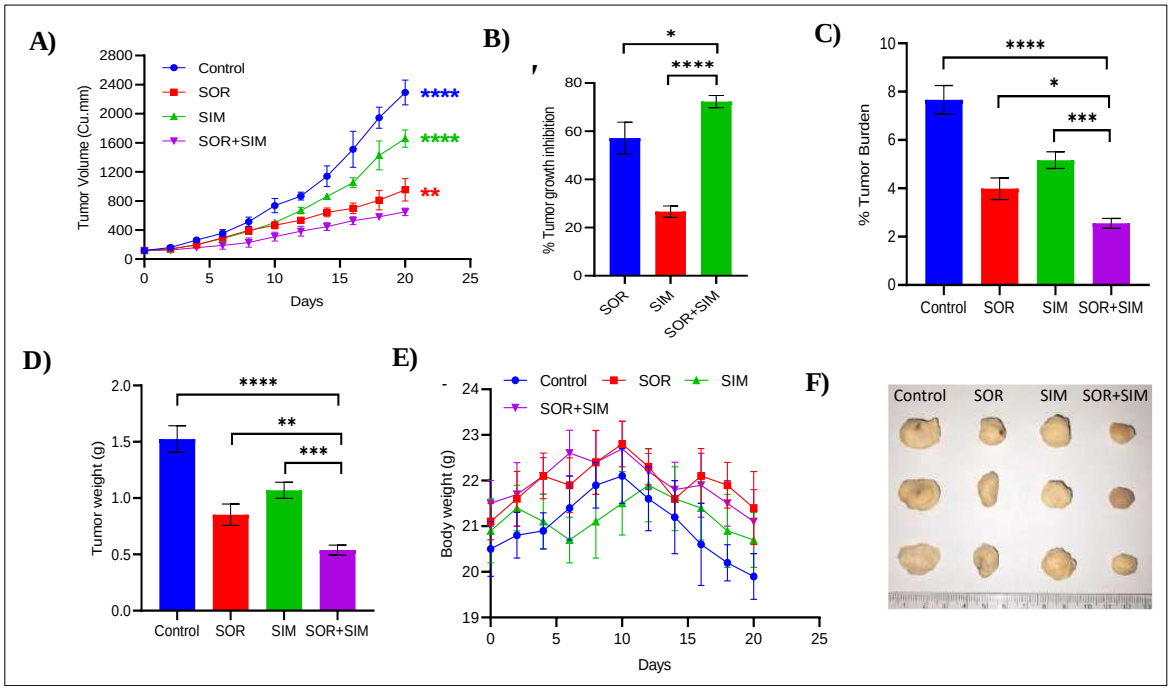

Figure 12: *In-vivo* anticancer activity (A-E) represents the tumor volume regression, % tumor inhibition rate, % tumor burden, tumor weight and observed body weight of the animals during the treatment course. Panel (F) represents the digital photograph of the representative tumors from the animals that were isolated at the end of the study. Here, *=P<0.05; **=P<0.01; ***=P<0.001 and ****=P<0.0001.

Publication:

Kaushik Kuche, Vivek Yadav, Meet Patel, Rohan Ghadi, and **Sanyog Jain**, Exploring sorafenib and simvastatin combination for ferroptosis-induced cancer treatment: Cytotoxicity screening, in vivo efficacy, and safety assessment. **AAPS PharmSciTech**, 2023 (In Press) **(Impact factor: 3.3)**

- **Brief Research report 3**

Exploring the synergistic behaviour of paclitaxel and vorinostat upon co-loading in albumin nanoparticles for breast cancer management

Paclitaxel (PTX) is a dynamic anticancer agent with a wide range of activity against various solid tumors, presently employed as a first-line anticancer drug in the treatment of breast cancer. However, the clinical success of PTX as a solitary therapeutic agent is ruined by its toxic side effects, low aqueous solubility, poor pharmacokinetics, poor tissue permeability, absence of tumor selectivity, and resistance due to efflux transporter. Additionally, marketed formulations of PTX and Taxol® often come with their own set of issues, including hypersensitivity and cytotoxic reactions. To overcome the drug resistance, minimize the toxic effects related to high-dose PTX and simultaneously maintain the therapeutic effect of PTX, synergistic combinatorial regimens such as epigenetic modulators have been employed to attain synergy in therapeutic outcomes over the individual drugs in breast cancer treatment. Vorinostat (VOR), one of the potential epigenetic modulators, has been reported to improve the anticancer efficacy of PTX in various cell lines such as endometrial, lung, ovarian, etc. by inhibiting pan-histone deacetylase. The treatment combining PTX and VOR could potentially bypass drug-resistant colonies generation and minimize drug resistance. Moreover, to achieve an improved/synergistic effect of PTX with VOR both drugs should reach the target site at the same time and therefore it becomes necessary to administer them by the same route, preferably in a single formulation. However, VOR has been shown to have limited action when used as a monotherapy in breast cancer management. To optimize the co-delivery of PTX and VOR and harness their synergistic effects, we designed PTX-and VOR-bound albumin nanoparticles (PTX-VOR-BSA-NPs). To ensure efficient drug loading, a modification was made to the process: the drugs were first allowed to bind with albumin for 24 h (as drugs take at least 16-18 h to bind with albumin at a molecular level) followed by desolvation to form albumin nanoparticles. Further stabilization was achieved by introducing glutaraldehyde as a crosslinking agent. The PTX-VOR-BSA-NPs were of 140 nm size, PDI around 0.18, and about 78% and 68% of entrapment efficiency for PTX and VOR, respectively. A bi-pattern release of both PTX and VOR was observed from PTX-VOR-BSA-NPs with a burst release for 2 h succeeded by sustained release till 24 h. PTX-VOR-BSA-NPs showed a higher apoptotic index (1.29) compared to free PTX (0.46) and VOR (0.39). Furthermore, PTX-VOR-BSA-NPs exhibited superior antitumor efficacy compared to PTX-BSA-NPs, which can be attributed to BSA's inherent self-targeting property and the synergistic action of PTX and VOR, resulting in a significant reduction in tumor volume compared to Intaxel®—a finding consistent with cell cytotoxicity and apoptosis assay results. PTX-VOR-BSA-NPs also demonstrated a more favourable PTX pharmacokinetic profile, with approximately a 1.4-fold improvement in AUC over Intaxel®. Moreover, toxicity biomarkers remained at similar levels to the control group. In summary, the developed PTX-VOR-BSA-NPs were found to have less toxicity and more effectiveness compared to the marketed formulation, thus affirming the generation of a potent as well as safe product.

Highlighted experimental outcomes:

Table 3: The IC_{50} values of Free PTX, Free VOR and PTX-VOR-BSA-NPs

Formulation	IC_{50} Value (ug/ml)
Free PTX	9.06
Free VOR	14.46
PTX-VOR-BSA NPs	2.075

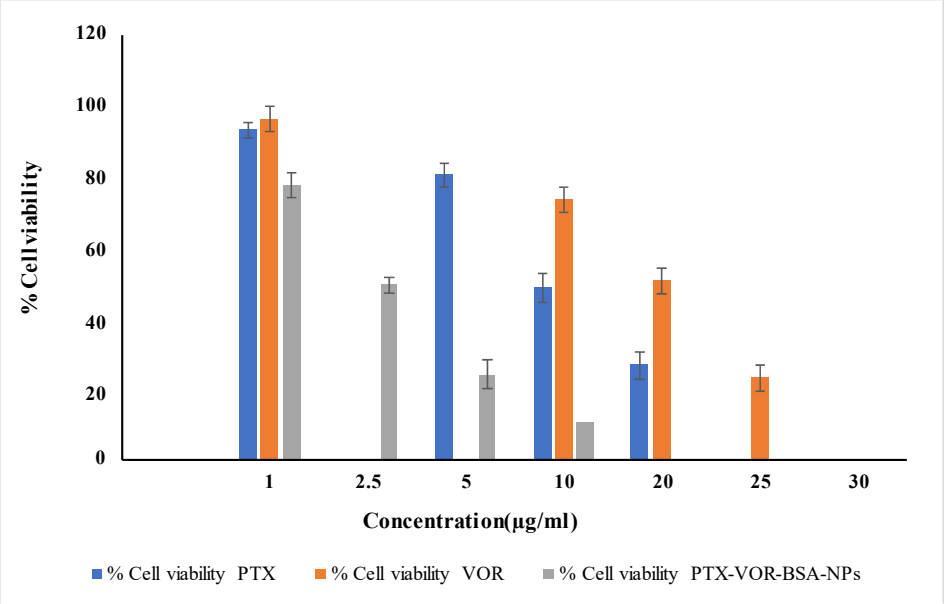

Figure 13: Graphical representation of cell cytotoxicity shown by free PTX, free VOR and PTX- VOR-BSA-NPs

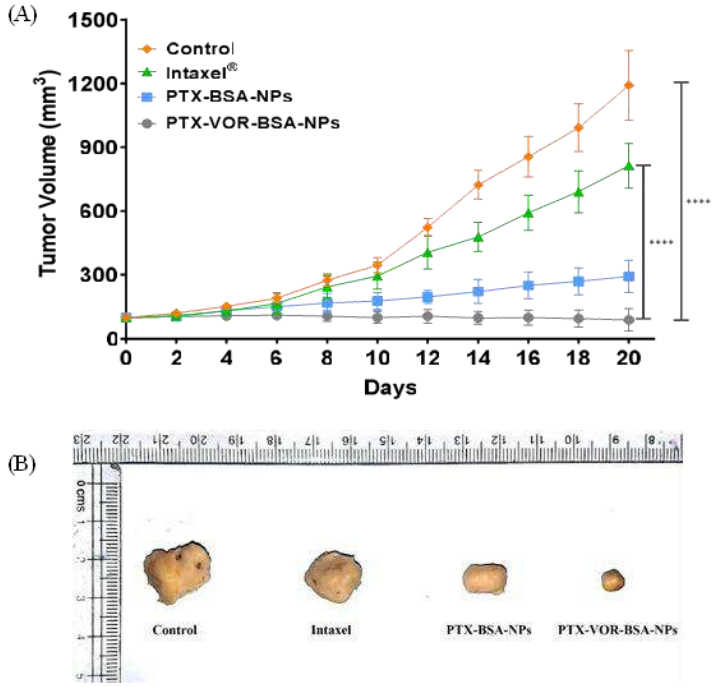

Figure 14: Graphical and pictorial illustration of tumor volume reduction. (A) Tumor volumes calculated at regular intervals, values are considered as mean ± SD (n=5); ****, statistical significance at $p < 0.0001$, and (B) Pictures of tumors after treatment with various formulations

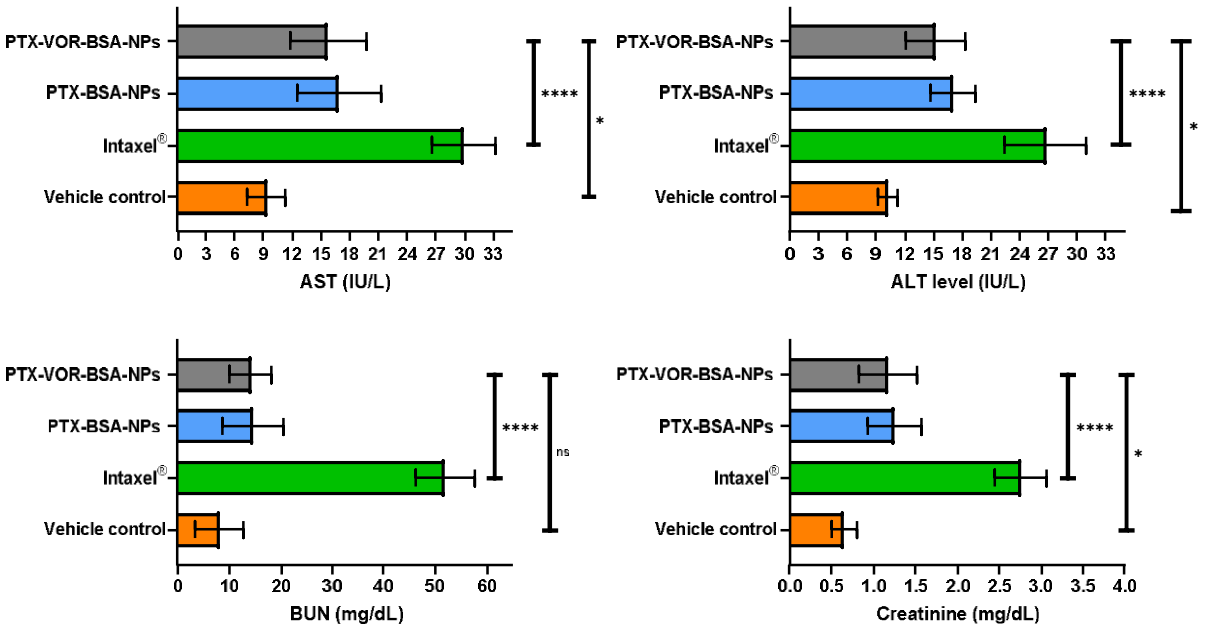

Figure 15: Graphical representation of the levels of hepatotoxic and nephrotoxic biomarkers in serum after treatment with different formulations. values are considered as mean ± SD (n = 5); ****, *, ns indicate statistical significance at $p < 0.0001$, $p > 0.01$, non-significant respectively.

Publication:

Ashwin Abhang, Oly Katari, Rohan Ghadi, Dasharath Chaudhari, **Sanyog Jain**, Exploring the synergistic behaviour of paclitaxel and vorinostat upon co-loading in albumin nanoparticles for breast cancer management. **Drug Delivery and Translational Research** (2023). https://doi.org/10.1007/s13346-023-01415-7 **(Impact factor: 5.4)**

- **Brief Research report 4**

pH sensitive liposomes assisted specific and improved breast cancer therapy using co-delivery of SIRT1 shRNA and Docetaxel

Docetaxel (DTX), a microtubule hyper stabilizing agent has been considered as the potent drug to treat breast cancer. DTX is commercially marketed as Taxotere®, which contains dehydrated alcohol (0.395 mg/mL) and high surfactant concentration (Tween 80) for achieving the desired solubility of DTX, which leads to multiple *in vivo* toxic reactions. Moreover, overexpression of SIRT1 in cancer cells stimulates the efflux transporter's expression along with multidrug resistance receptors, leading to the decreased therapeutic efficacy of DTX. This enables cells to exhibit hyper-proliferation and anti-apoptotic rewards and encourages DNA damage repair. Thus, the integration of bio-therapeutics with DTX, capable of suppressing SIRT1 production and barring the expression of efflux transporter, holds the potential for elevating the therapy standards. Numerous studies have highlighted that within bio-therapeutics, shRNA exhibits lesser off-target effects with multiple target silencing capability and superior efficiency when compared to other nucleic acid-based therapeutics. These advantages of shRNA, make them a better therapeutic candidate than siRNA and certainly a better contender for future investigations. Further, a compelling

delivery system may enhance the response and can also assist in the development of next-generation cancer therapeutics. The majority of researchers have attempted to enhance the targeted delivery of genes to tumor cells by employing either novel lipids or active ligands to improve the issues pertaining to their low transfection efficiency, systemic stability, and lack of endosomal escape. Moreover, even after active targeting, the effective release of cargo from endosomes remains to be a challenge. So, designing a smart nano-vesicular system with the ability to co-deliver a bio-therapeutic molecule along with a DTX is what is ideally desired for effective cancer management. Hence, in the present investigation, we developed a novel SIRT1 silencing RNA (SIRT1 shRNA) and DTX co-loaded pH-sensitive lipoplex (DTX-lipoplex), aiming to explore their synergistic potential for enhancing breast cancer treatment and reducing the toxicity of the formulation. The DTX-lipoplex were prepared by solvent evaporation and rehydration method and were evaluated for various quality attributes (particle size, % entrapment efficiency, hemotoxicity, DNA stability efficiency etc.), in vitro drug release, cell culture assays, antitumor efficacy, and in vivo toxicity. The DTX-lipoplex showed a substantial synergistic effect, reducing the IC_{50} by approximately ~2.35 fold and ~2.54 fold in comparison to DTX alone, in MDA-MB-231 and MCF-7 cells respectively. This was due to the higher internalization of the corresponding formulation in cells because of their pH-sensitive properties. Furthermore, DTX-lipoplex showed ~3-fold higher DTX titre within the tumor cells thereby significantly reducing the tumor burden (~78%) when compared to the marketed non pH sensitive lipid transfection agent and clinical counterpart i.e., Taxotere®, showcasing the synergistic potential of DTX-lipoplex in both tumor reduction and animal survival. Despite the lower concentration of DTX, better anti-tumor efficiency was induced due to the synergistic effect of shRNA. Furthermore, DTX-lipoplex exhibited low hemo-, hepato- and nephro-toxicity. These findings corroborated the rational of exploring co-delivery of DTX and shRNA, which could improve the limited efficacy of DTX monotherapy. Thus, to conclude it can be said that co-delivering DTX and SIRT1 shRNA in a single tumor-specific nano-platform can improve the therapeutic potential of current therapy.

Highlighted experimental outcomes:

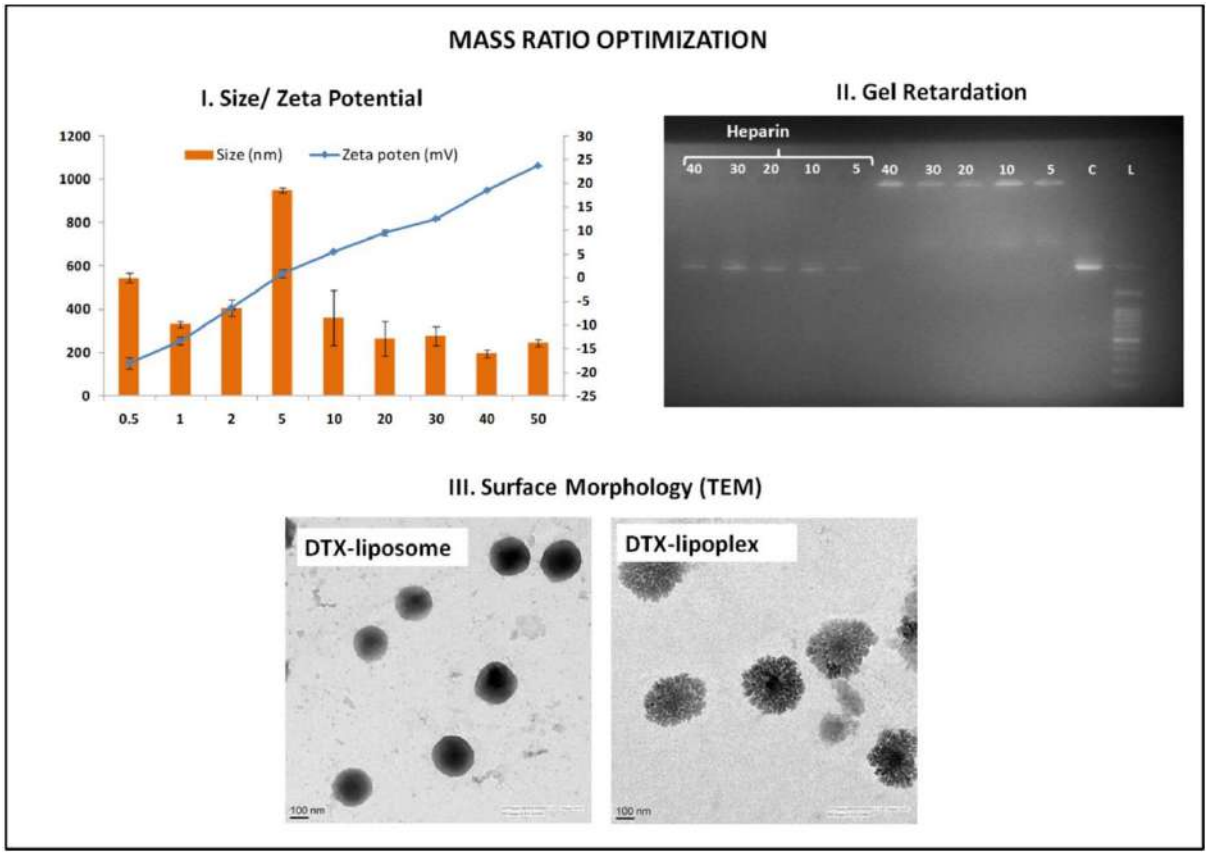

Figure 16: Optimization of the DTX-lipoplex; (I) size/zeta potential with respect to mass ratio of the lipoplex; (II) gel retardation analysis/heparin displacement studies; (III) surface morphology of the DTX-liposome and DTX-lipoplex using TEM.

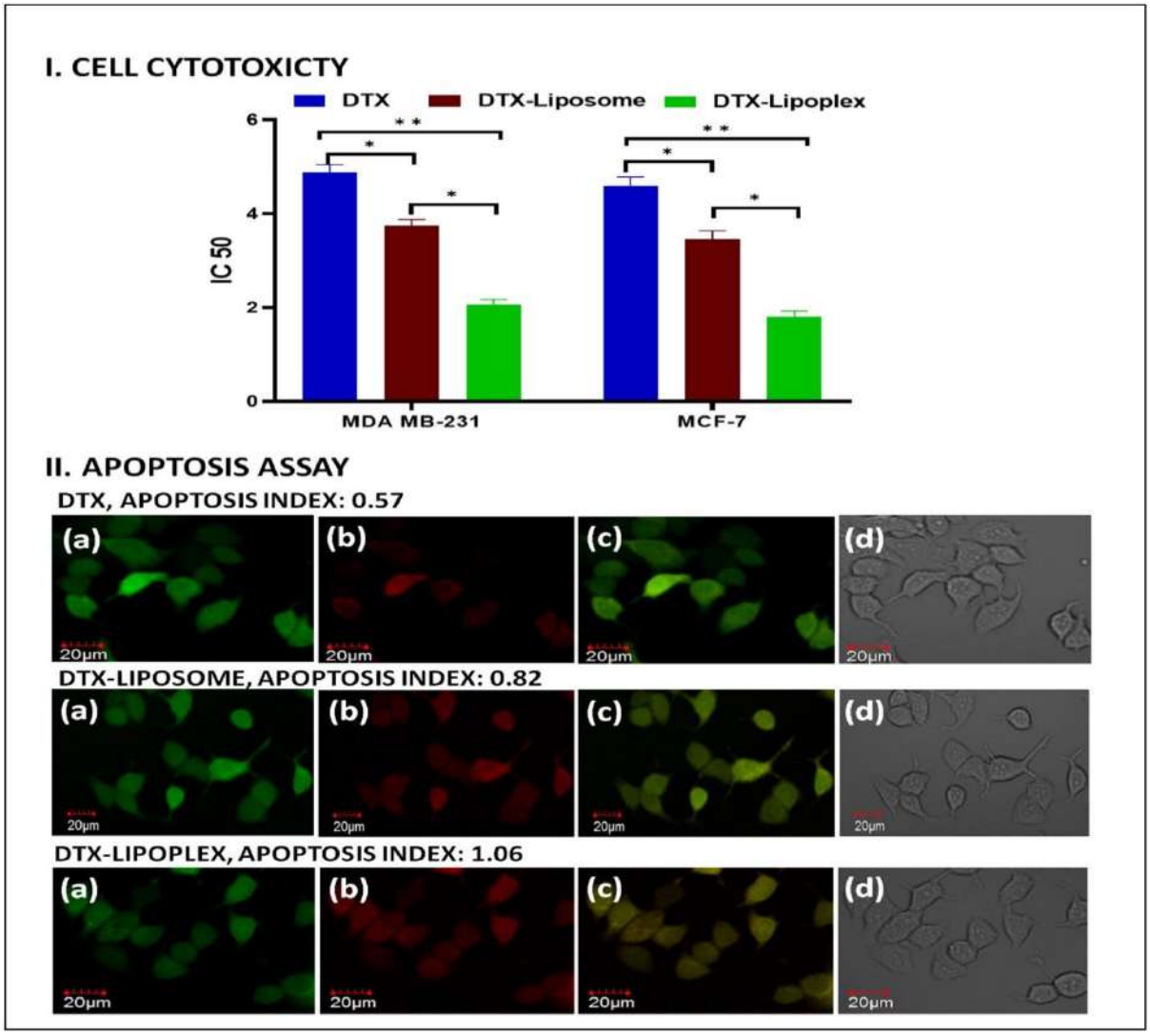

Figure 17: *In vitro* cell cytotoxicity assay. I. IC_{50} obtained from cell cytotoxicity assay; II. apoptosis assay of free DTX, DTX-liposome and DTX-lipoplex in MCF-7 cells; (a) green channel and (b) red channel depicts the fluorescence from carboxy fluorescein (cell viability marker dye) and fluorescence from Annexin Cy3.18 conjugate (cell apoptosis marker dye) respectively; (c) third channel depicts the overlay; (d) fourth represents the differential contrast image of representative cells

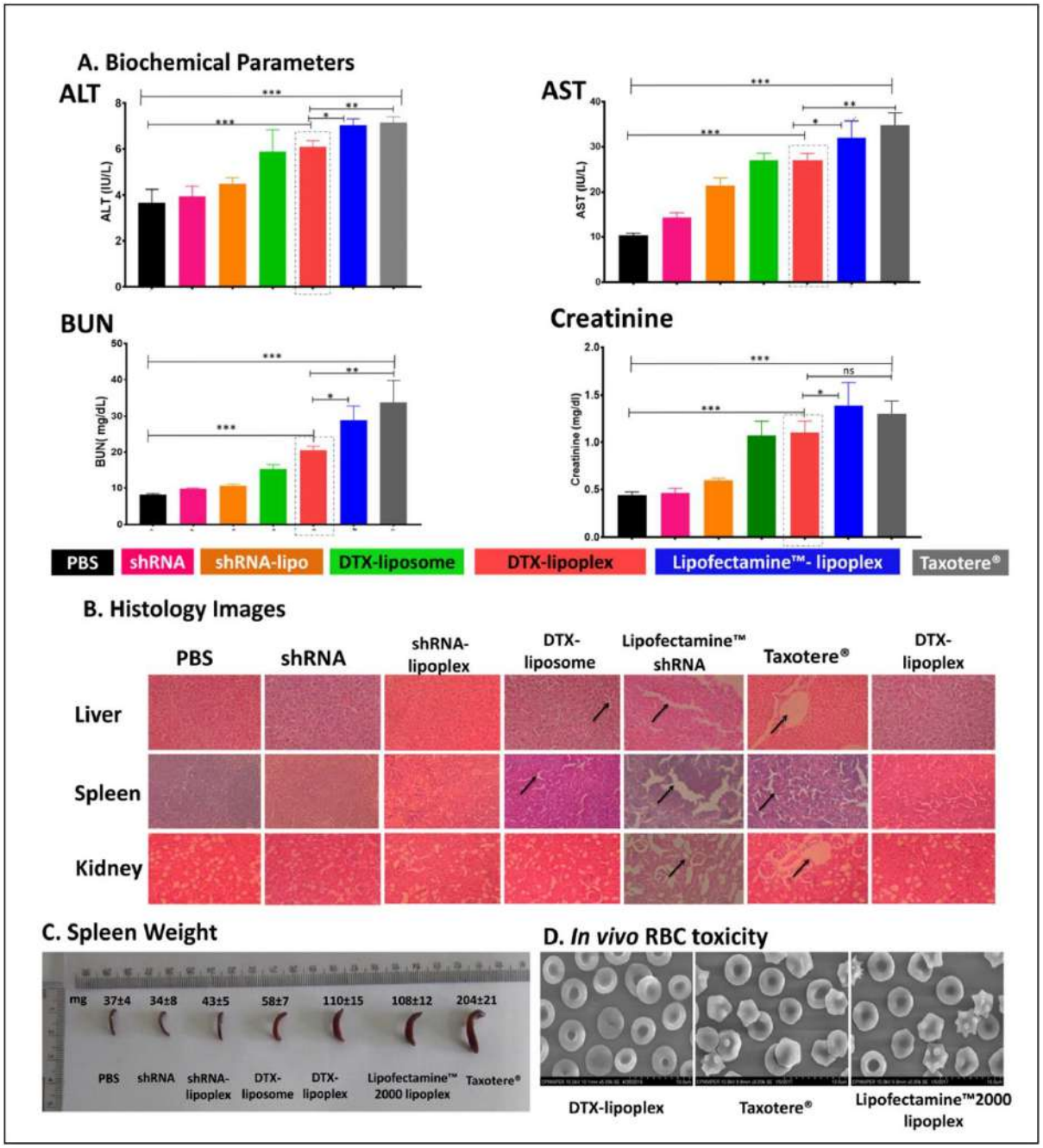

Figure 18: *In vivo* toxicity evaluations using different techniques A. Biochemical parameters assessed in serum indicating changes in the hepatic and kidney biochemical parameters after 7 days treatment with formulations; B. histology Images of different vital organs such as kidney, spleen, and liver sections respectively; C. spleen weight as representation of the *in vivo* toxicity caused by formulation treatments: D. *in vivo* hemocompatibility illustrated by SEM images of RBC's.

Publication:

Rajan Swami, Yogesh Kumar, Dasharath Chaudhari, Sameer S. Katiyar, Kaushik Kuche, Parmeshwar B. Katare, Sanjay K. Banerjee, **Sanyog Jain**, pH Sensitive Liposomes Assisted Specific and Improved Breast Cancer Therapy using codelivery of SIRT1 shRNA and Docetaxel. **Materials Science and Engineering C: Mater Biol Appl**, 120, 2021: 111664 **(Impact factor: 7.9)**

- **Brief Research report 5**

Chemosensitizer and docetaxel-loaded albumin nanoparticle: overcoming drug resistance and improving therapeutic efficacy

DTX, a widely used chemotherapeutic agent, has demonstrated remarkable efficacy in treating various cancers, including breast cancer. However, its effectiveness is often hindered by the overexpression of drug efflux transporters such as P-glycoprotein (P-gp), breast cancer resistance protein (BCRP), and ATP-dependent efflux transporters. These cellular gatekeepers actively pump out DTX and other chemotherapeutic drugs, leading to reduced intracellular drug concentrations and, consequently, treatment resistance. Furthermore, it leads to severe side effects, including acute hypersensitivity reactions, fluid retention, neurotoxicity, febrile neutropenia, nail toxicity, myalgia, and nasolacrimal duct stenosis. To address these challenges, researchers have explored the potential of bioactive compounds derived from plants, such as piperine, curcumin, naringenin, and tariquidar, as chemosensitizers. These compounds have shown promise in reversing chemoresistance by simultaneously modulating multiple pathways involved in tumorigenesis. Quercetin (QT), a potent chemosensitizer, possesses a wide range of therapeutic benefits, including apoptosis induction, angiogenesis inhibition, and efficacy against various human carcinoma cells. QT has also demonstrated antioxidant activity, mitigating oxidative stress and mutagenesis. Importantly, QT interacts with P-gp, effectively suppressing its activity by downregulating P-gp and other transporters like MRP1 and BCRP in a dose-dependent manner. Therefore, our current investigation attempts to develop an i.v. bolus DTX and QT co-loaded albumin nanoparticles (DTX–QT–BSA NPs), with the goal of overcoming drug resistance and enhancing therapeutic effectiveness through the synergistic potential of these two agents. BSA–NPs containing both drugs were optimized, extensively characterized for different quality attributes and performance was investigated using series of in vitro and in vivo investigations. BSA–NPs loaded with a 7 wt % of DTX and 3 wt % of QT corresponding to their molar ratio were formulated to employ this synergy. The observed elevated fluorescence inside MDA MB-231 cells, ordered as free Rho < mixture of free Rho and QT < Rho-DTX-QT-BSA-NPs and Rho-DTX-BSA-NPs, likely stems from QT's potential to inhibit P-gp efflux. Among all formulations, DTX-QT-BSA-NPs showed the highest apoptotic potential (apoptotic index: 1.03) compared to other formulations, including DTX-BSA-NPs (0.92) and pure drugs (0.54 for free DTX, 0.23 for free QT, and 0.52 for their mixture), indicating strong synergism as QT is reported to have anticancer activity by inhibiting EGFR and inhibits expression of the antiapoptotic gene Bcl-2. Tumor regression studies also highlighted the similar fact where DTX–QT–BSA–NPs significantly reduce the tumor burden (∼67%) than their counter parts (∼50% in DTX–BSA–NPs and ∼20% reduction in Docepar). Therefore, this BSA–NPs platform can open a window for the study of the synergistic effects between chemotherapy drugs and chemosensitizer drugs and to maximize therapeutic efficacy.

Highlighted experimental outcomes:

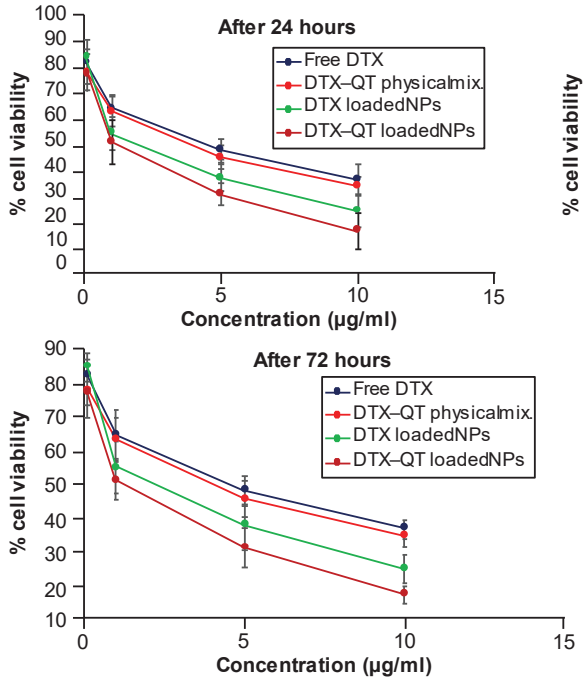

Formulations	IC_{50} value (µg/ml)		
	24 h	48 h	72 h
Free DTX	5.68	4.01	2.96
Free QT	65.74	45.31	21.96
DTX–QT physical mix.	3.96	2.90	1.96
DTX–BSA–NPs	3.31	2.32	1.33
DTX–QT–BSA–NPs	**2.31**	**1.76**	**0.71**

Figure 19: Cell cytotoxicity of various formulations after 24, 48 and 72 h (values are mean ± standard deviation, n = 5). Table highlights the IC_{50} obtained after exposure of the cell line with respective formulation after definite time. BSA: Bovine serum albumin; DTX: Docetaxel; NP: Nanoparticles; QT: Quercetin.

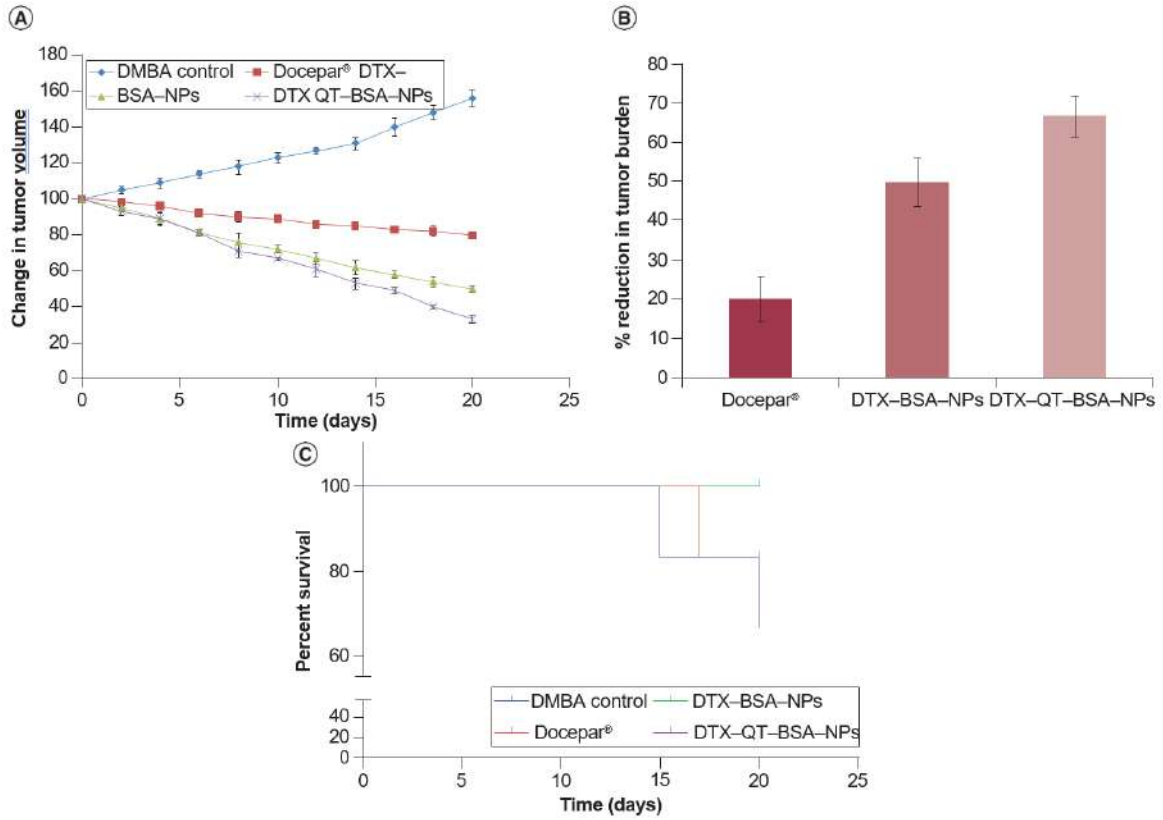

Figure 20: Tumor regression studies. (A) Change in the tumor volume; (B) reduction in tumor burden; (C) Kaplan–Meier survival analysis. BSA: Bovine serum albumin; DMBA: 7,12-dimethylbenz[a]anthracene; DTX: Docetaxel; NP: Nanoparticles; QT: Quercetin.

Figure 21: Images of tumor lobes after treatment with DTX formulations after termination of the study. × denotes the death of animals before termination of the study, hence tumor was not included in the study. BSA:Bovine serum albumin; DTX: Docetaxel; NP: Nanoparticles; QT: Quercetin

Publication:

Jagdish P. Desale, Rajan Swami, Varun Kushwah, Sameer S. Katiyar, **Sanyog Jain**, Chemosensitizer and Docetaxel Loaded Albumin Nanoparticle: Overcoming Drug Resistance and Improving Therapeutic Efficacy. **Nanomedicine**, 13(21), 2018: 2759-2776 **(Impact factor: 5.5)**

- **Brief research report 6**

Co-delivery of docetaxel and gemcitabine using bio-macromolecules based novel nanoformulations: An approach for synergistic dual drug therapy of cancer using a combinatorial therapeutic regimen

The combination of docetaxel (DTX) and Gemcitabine (GEM) is well tolerated and FDA-approved combination therapy for advanced, metastatic non-small-cell lung cancer and metastatic breast cancer. Gemcitabine (GEM) is an inactive analogue of nucleoside deoxycytidine, and its active diphosphate metabolite caused the termination of DNA chain synthesis. On the other hand, DTX promotes apoptosis leading to inhibition of mitotic and interphase cellular activity. The synergistic antitumor activity of GEM and DTX is attributed to their distinct mechanisms and partially non-overlapping toxicity. GEM is highly hydrophilic (water solubility of ~83 mg/ml) with a short half-life of 32–84 min as it rapidly decomposes into uracil metabolite 2′-deoxy-2′,2′-difluorouridine (dFdU). To achieve the desired therapeutic level, frequent administration is required which culminates in dose-dependent toxicity. Similarly, the hydrophobic nature of DTX forces the utilization of tween 80 and ethanol as a solubilizer and co-solvent respectively for its clinical application. For

example, the marketed formulation of DTX (Taxotere®) causes severe hypersensitivity reactions and requires the administration of dexamethasone to suppress the immune response in patients. Despite the positive outcome, the poor physicochemical properties and pharmacokinetic profile of DTX and GEM put forth a major challenge in the delivery and clinical utilization of this combination. Hence, the proposed work summarizes the two approaches to deliver this therapeutic combination (GEM and DTX) to improve the efficacy of cancer therapeutics as shown in figure 22.

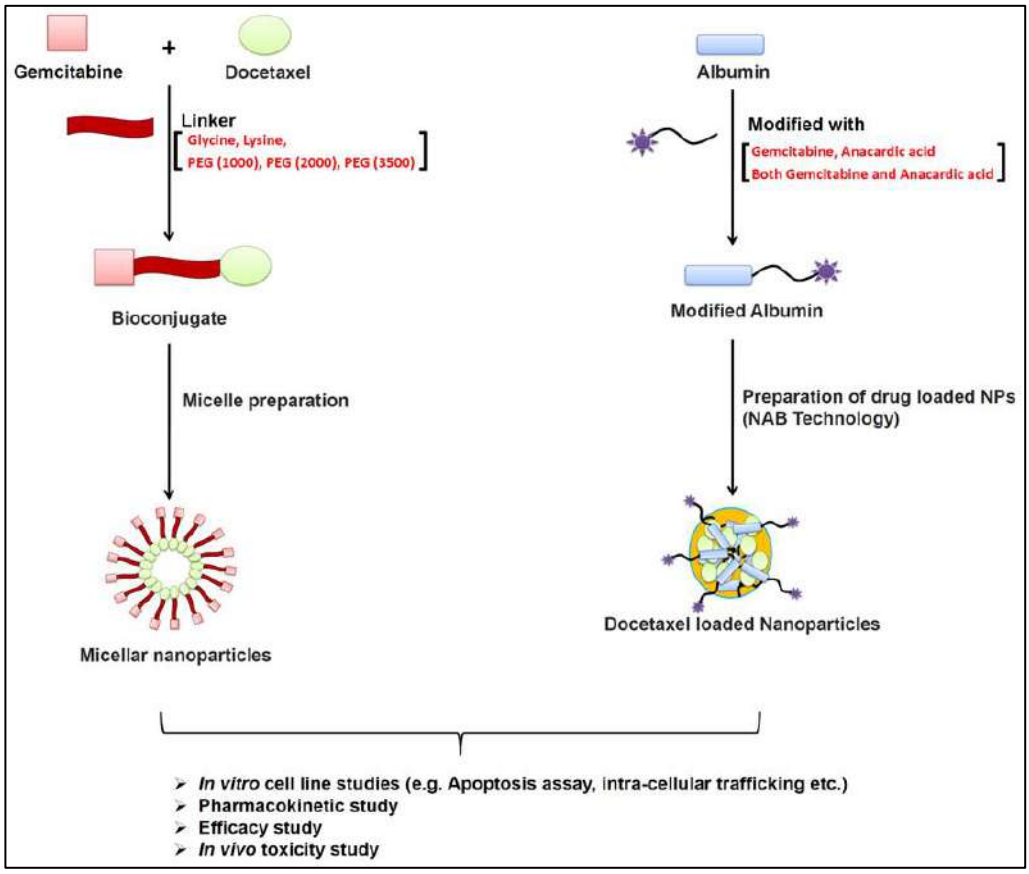

Figure 22: Proposed formulation strategies (micellar nanoformulation and albumin nanoformulation based) for co-delivery of GEM and DTX

A] **Covalent bonding of two GEM-DTX via linker group to form bioconjugate and assembly into a micellar structure.**

The investigation reported the effect of various linkers like short-length (glycine and lysine) and long-length linkers (PEG1000, PEG2000, and PEG3500) on pharmacokinetics and toxicity of DTX and GEM bio-conjugates. Conjugates were synthesized via carbodiimide chemistry and were characterized by ^{1}H-NMR and FTIR. The bio-conjugate was developed using long-length linkers that exhibited higher toxicity as compared to free drug congeners. Among the long-length linkers, DTX-PEG2000-GEM exhibited higher cellular cytotoxicity. Hence, suggesting PEG2000 as an optimal linker for enhancing the therapeutic efficacy of drug-polymer conjugate. Additionally, free GEM showed rapid degradation into inactive metabolite whereas conjugates with short-length linkers and long-length linkers demonstrated extended plasma stability of GEM conjugates owing to their stability against enzyme degradation. Introduction of PEG spacer as a linker for a fusion of drug molecules of

contrasting lipophilicity to achieve optimum hydrophilic and lipophilic balance. This property allows the conjugate to self-assemble and form micelles. The micelles forming capacity of DTX PEG2000-GEM was determined by fluorescence spectroscopy. The Critical micellar concentration (CMC) of the conjugate was found to be in the range of 7.83 μg/ml. Morphological characterization showed the spherical shape with two regions showing an inner dark and outer light circle validating the formation of a self-assembled structure-based alignment of the hydrophilic and hydrophobic moiety. The release behavior of conjugate was studied by *in vitro* hydrolysis experiment revealed sustained and higher release in acidic media (5.5 and 6.8) due to higher cleavage of bonds in weak acid. Intracellular uptake and subsequent intracellular trafficking of free drugs (GEM, DTX) and micelles demonstrated enhanced internalization and formation of lysosomes in GEM-PEG2000-DTX micelles as compared to free drugs. The dependence of micelles on OATP1B3 and hNTs transporter for internalization was studied using dipyridamole as an inhibitor of this transporter. The result showed a significant increase in IC_{50} value in free drug and combination as compared to control without inhibitors. Furthermore, qualitative estimation of apoptosis was performed by Annexin-V assay demonstrating a higher apoptosis rate of DTX-PEG2000-GEM with respect to free drugs and combination. This may be due to higher clathrin-mediated cellular uptake and retention. The comparison of the safety profile of the marketed formulation (Taxotere and Gemzar) and developed DTX-PEG2000-GEM showed insignificant hemolysis when compared with the control (PBS), whereas higher hemolytic activity was observed in the marketed formulation. *In vivo* pharmacokinetic profile of micelles revealed an increase in $AUC_{(0-\infty)}$ and $t_{½}$ of GEM when compared with the marketed formulation Gemzar. This might be ascribed to the stealth property of PEG polymer. *In vivo* pharmacodynamic study showed a significant reduction in tumor burden of DTX-PEG2000-GEM with respect to the marketed formulation (Gemzar®, Taxotere®). The improved pharmacodynamic efficacy was observed due to enhanced retention and permeation phenomenon demonstrating the selective delivery of NPs in tumor vicinity. Moreover, the Kaplan-Meier survival curve demonstrated increased survival of animals with tumor, when treated with DTX-PEG2000-GEM, compared to DMBA control and marketed formulation, indicating the safety of the developed formulation. Comparative evaluation of toxicity between the marketed formulation and DTX-PEG2000-GEM revealed a significant increase in the level of hepatotoxicity markers such as AST, and ALT and nephrotoxicity markers like BUN and creatinine in the marketed formulation, whereas there was an insignificant difference in levels when compared with control animals. The reduced toxicity of micelles is due to the absence of solvent-mediated toxicity which is a major contributing factor in marketed formulation. Finally, the safety profile was further validated through histopathological examination of the liver, kidney, and spleen. Evidently, the marketed formulation exhibited higher toxicity which was evident from the severe inflammation and reduced tissue density in the case of the marketed formulation.

Highlighted experimental outcomes:

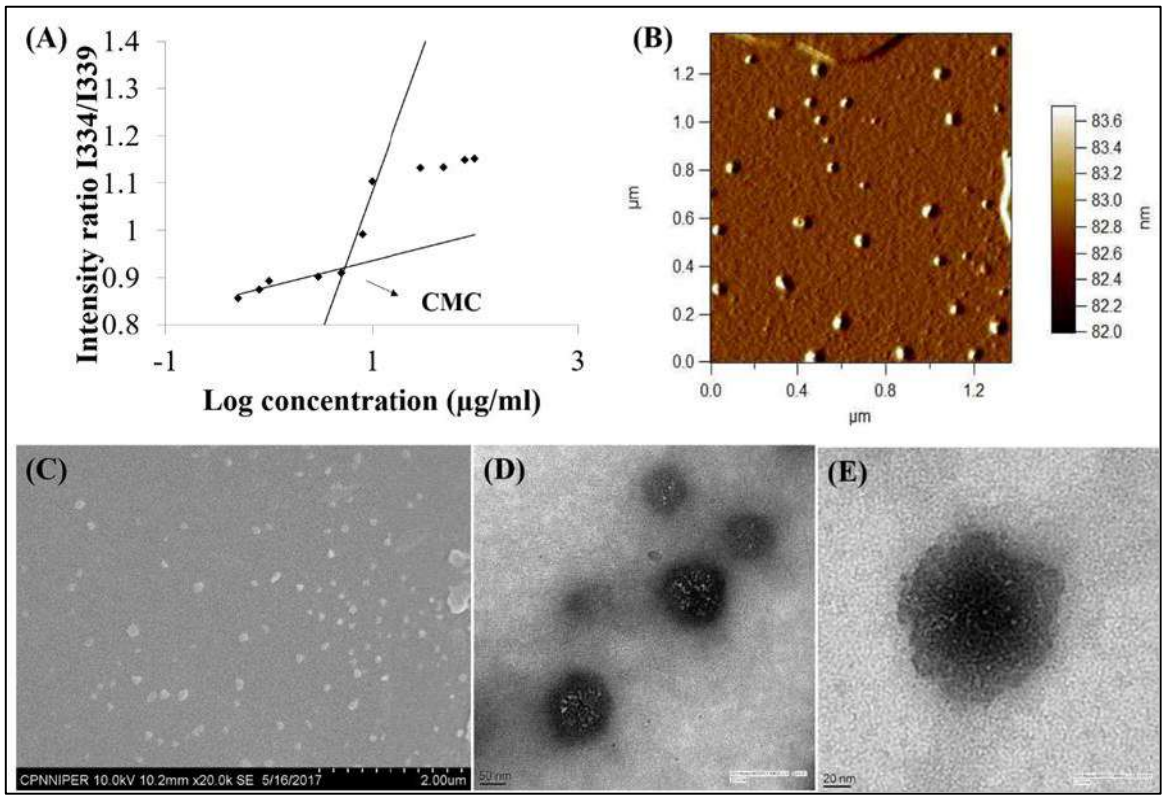

Figure 23: (A) CMC determination of DTX-PEG-GEM NPs; Surface morphology analysis via (B) AFM (C) SEM and (D) TEM. (E) Single particle TEM image of DTX-PEG-GEM NPs.

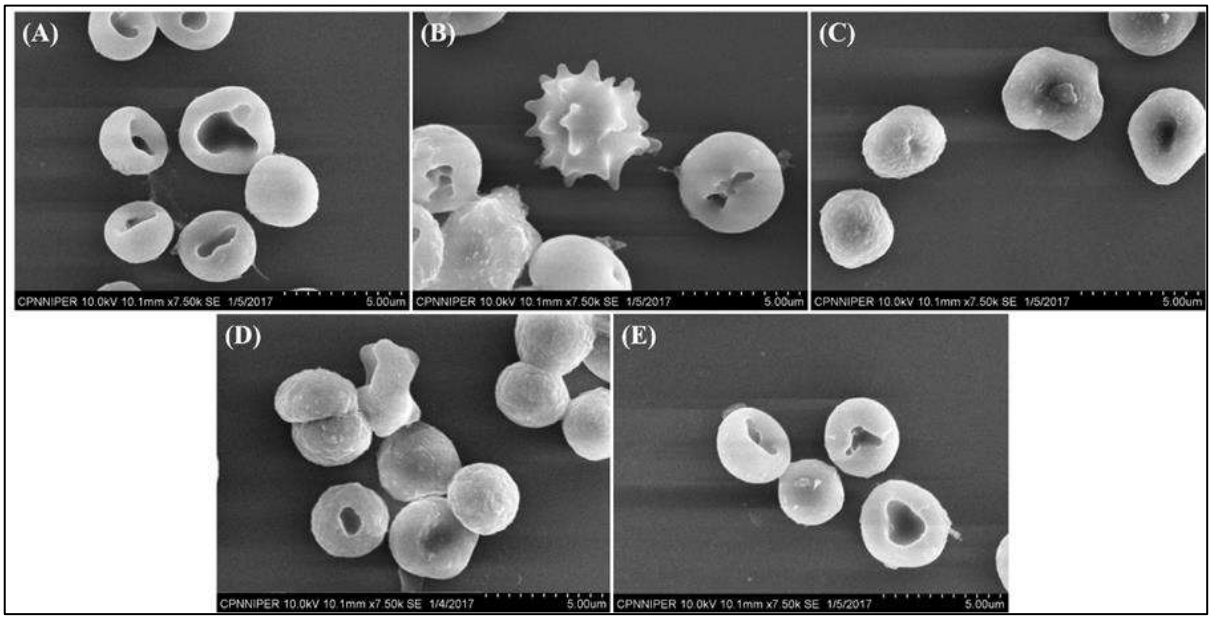

Figure 24: SEM micrographs of RBCs indicative of (A) control and different groups treated with (B) Gemzar®, (C) Taxotere®, (D) Gemzar® + Taxotere®, (E) DTX-PEG-GEM NPs

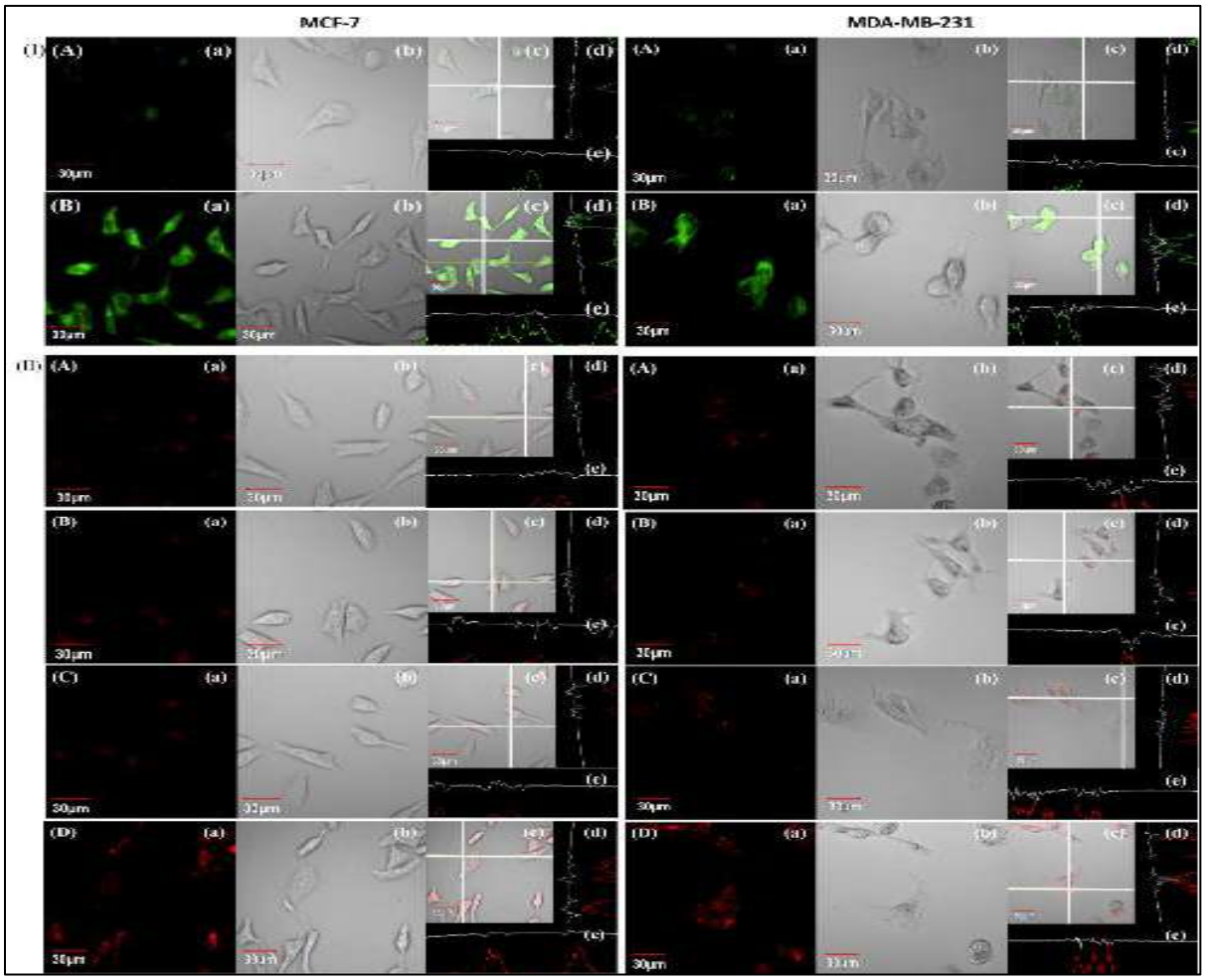

Figure 25: (I) Cellular uptake of (A) free C-6 and (B) C6-NPs in MCF-7 and MDA-MB-231 cells. (a) Green fluorescence of C-6. (b) Corresponding DIC images (c) overlay of a and b and (d and e) vertical and horizontal line series analysis long the white line of image c; (II) Intracellular fate of (A) free GEM, (B) free DTX, (C) combination of free DTX+GEM and (D) DTX-PEG-GEM NPs shown by staining with LysoTracker Red in MCF-7 and MDA-MB-231 cell lines. (a) Red fluorescence of LysoTracker; (b) Corresponding DIC images (c) Overlay of a and b; (d and e) vertical and horizontal line series analysis of fluorescence along the white line of c; and (*) and (**) depicts green fluorescence of C-6 loaded DTX-PEG-GEM NPs and overlay of panel a and *, respectively.

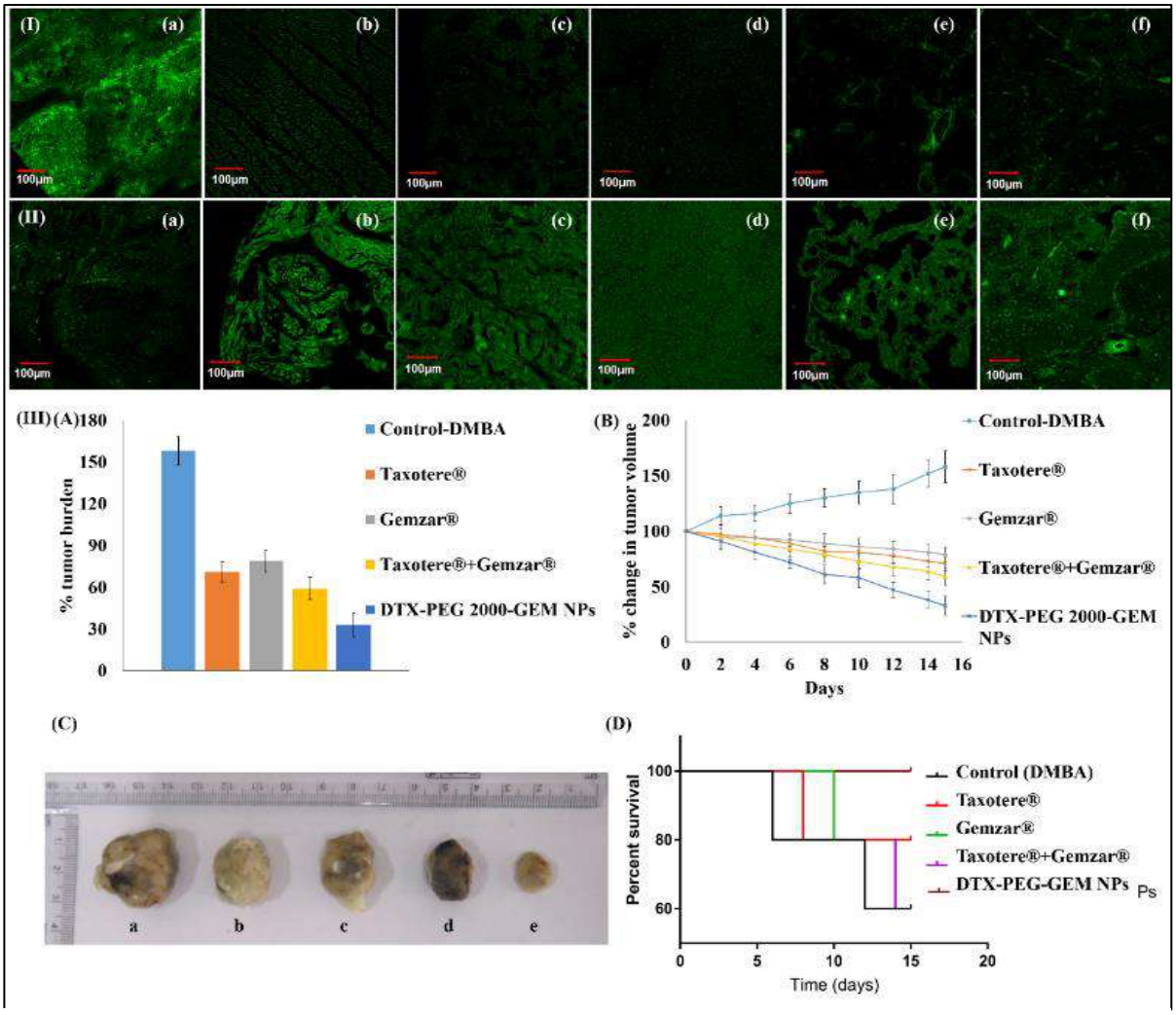

Figure 26: Fluorescence intensity of (I) C-6 loaded DTX-PEG-GEM NPs, (II) Free C-6 and (III) (A) % tumor burden in animals treated with different formulations; *** (significant difference at $p < 0.001$) w.r.t. a (control), b (Taxotere®), c (Gemzar®) and d (Taxotere® + Gemzar®) (B) Comparison of % change in tumor volume (C) Representative photographs of excised tumors from (a) Control, (b) Taxotere®, (c) Gemzar®, (d) Taxotere® + Gemzar® and (e) NPs treated groups and (D) Kaplan–Meier survival curve depicting the survival rate of tumor-bearing animals received different treatments

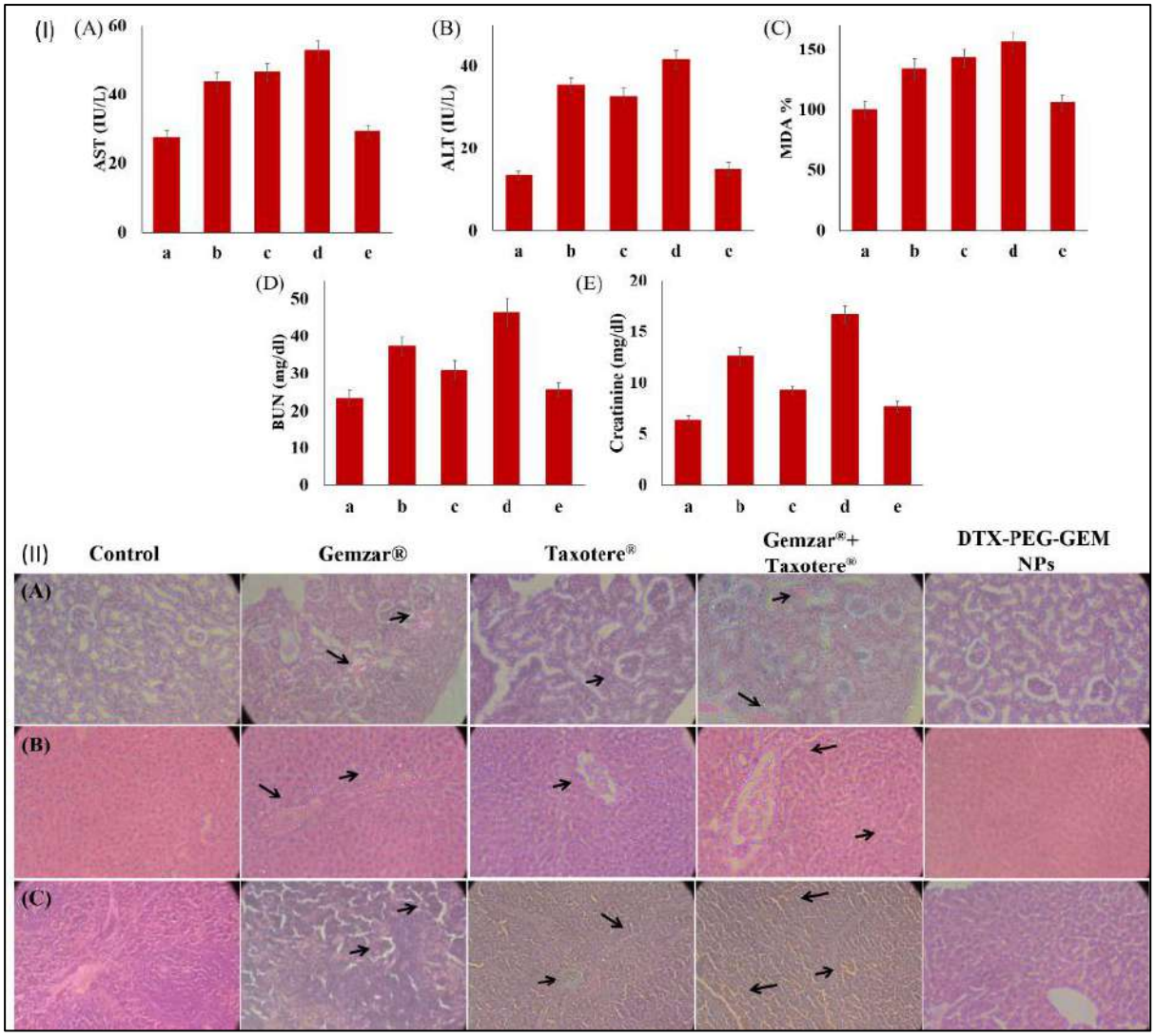

Figure 27: (I) Biochemical markers (A) AST (B) ALT (D) BUN (E) creatinine levels in plasma and (C) MDA level in liver homogenate after 7 days following administration of (b) Gemzar®, (c) Taxotere®, (d) Gemzar® + Taxotere® and (e) DTX-PEG-GEM NPs as compared to (a) control. ***, significant difference at $p < 0.001$; ns, insignificant. Values are expressed as Mean ± SD (n = 5); (II) Histopathological sections of (A) kidney, (B) liver, and (C) spleen following the treatment with individual drugs, their combination, and developed NPs.

B] **Conjugating GEM with albumin and targeting moiety to impart hydrophobicity and enhanced interaction and subsequently loading hydrophobic drug DTX.**

The hydrophilic property of GEM can be modified by conjugating it with Bovine Serum Albumin (BSA). Conjugation with albumin increases the stability against deamination from cytidine deaminase (CDA) through the formation of a hydrolysable amide linkage. Despite an increase in stability, there is a remarkable increase in hydrophilicity of albumin which leads to a decrease in affinity towards DTX. To regain the hydrophilic and hydrophobic balance of albumin, hydrophobic anacardic acid (AA) was conjugated to BSA. Furthermore, conjugate AA-GEM BSA is formulated into NPs to enhance the solubility of DTX. The presence of AA is anticipated as a targeting agent as it possesses affinity towards VEGF receptors which are generally overexpressed in tumor angiogenesis.

In the present study, AA-GEM-BSA conjugate was synthesized by using TDC/NHS carbodiimide chemistry and was further characterized by ^{1}H NMR and FTIR. The synthesized conjugate was used for the preparation of nanoparticle NPs by high-pressure homogenization. The SEM and AFM analysis of AA-GEM -BSA NPs confirmed the formation of a spherical shape. The PXRD spectra of NPs demonstrated the absence of characteristic peaks of DTX and GEM showing an amorphous form of drugs in NPs. *In vitro* drug release studies showed significant retardation of DTX release from AA-GEM-BSA NPs. Moreover, there was a higher amount of the release of GEM in pH 5.5 of the tumor microenvironment. Cellular uptake and nuclear co-localization assay were performed on MCF-7 and MDA-MB-231 cell line showed significantly higher cellular uptake and nuclear co-localization demonstrated via box and line series analysis of AA-GEM-BSA NPs in comparison with unmodified NPs. The intracellular fate of NPs revealed the endocytic uptake of NPs through the endo-lysosomes pathway. The hepatotoxicity and nephrotoxicity of AA-GEM-BSA were analyzed by using hepatotoxicity biomarkers like BUN and creatinine and nephrotoxic biomarkers like AST, and ALT. No significant difference in the level of biochemical parameters of DTX-loaded AA-GEM -BSA NPs in comparison with a marketed formulation of DTX and GEM. The result of histopathological studies was in line with the biomarker study. Further, there was no noticeable change in the morphology of the RBC incubated with DTX-loaded AA-GEM-BSA NPs. *In vivo* antitumor efficacy study demonstrated the significant suppression of tumor growth. After 15 days of treatment, tumor size was reduced by about 35.72% in the case of DTX-loaded AA-GEM-BSA NPs as compared to the control group.

Highlighted experimental outcomes:

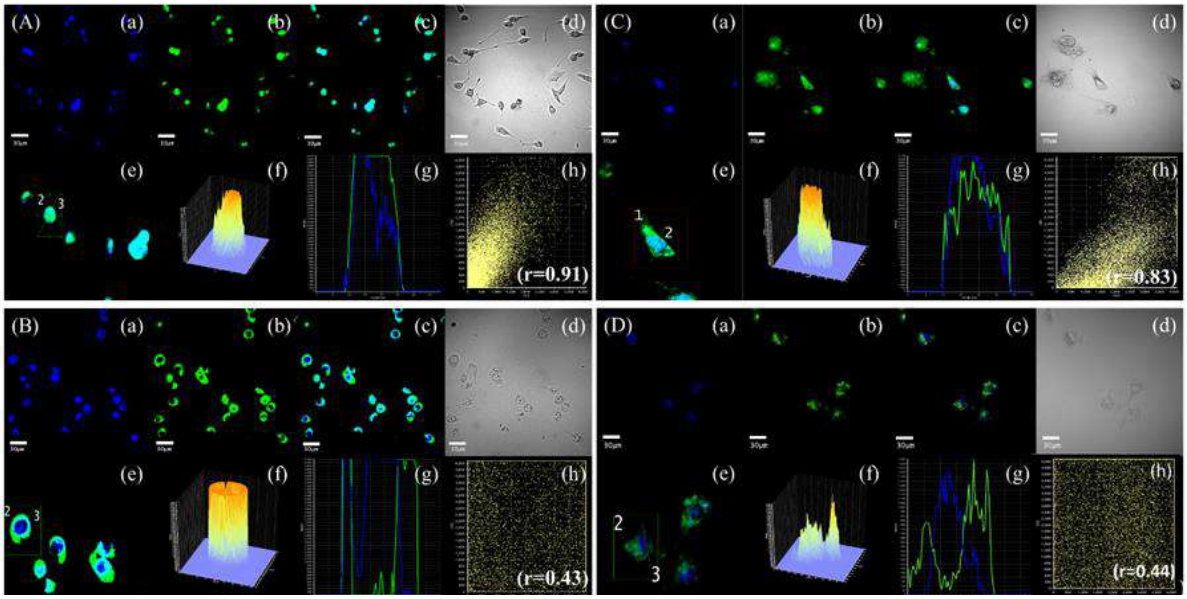

Figure 28: Confocal images of MCF-7 cells incubated with (A) AA-GEM-BSA NPs, (B) BSA NPs, MDA-MB-231 cells incubated with (C) AA-GEM-BSA NPs, (D) BSA NPs. Panel a and b represent the DAPI-stained nucleus and C-6 loaded NPs in the same cells, respectively and panel c reflects the overlay images of panels and b. Panel d shows a DIC image of the treated cells, and panel e represents high resolution images of panel c. The box analysis (f) line analysis plots (g), and scatter plot analysis (h) show interaction of DAPI and C-6. Scale bar denotes 30 μM.

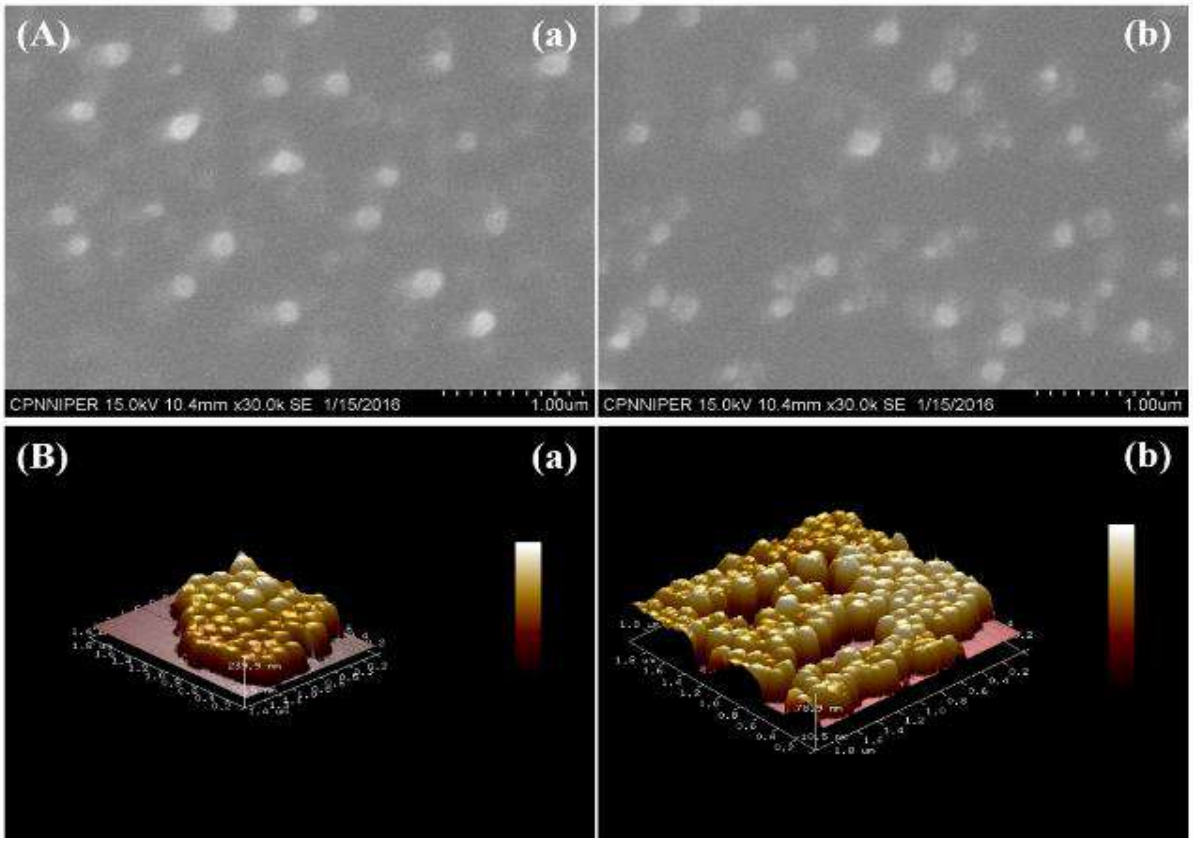

Figure 29: Surface morphology analysis via (A) SEM image (B) AFM image of (a) BSA NPs and (b) AA-GEM-BSA NPs

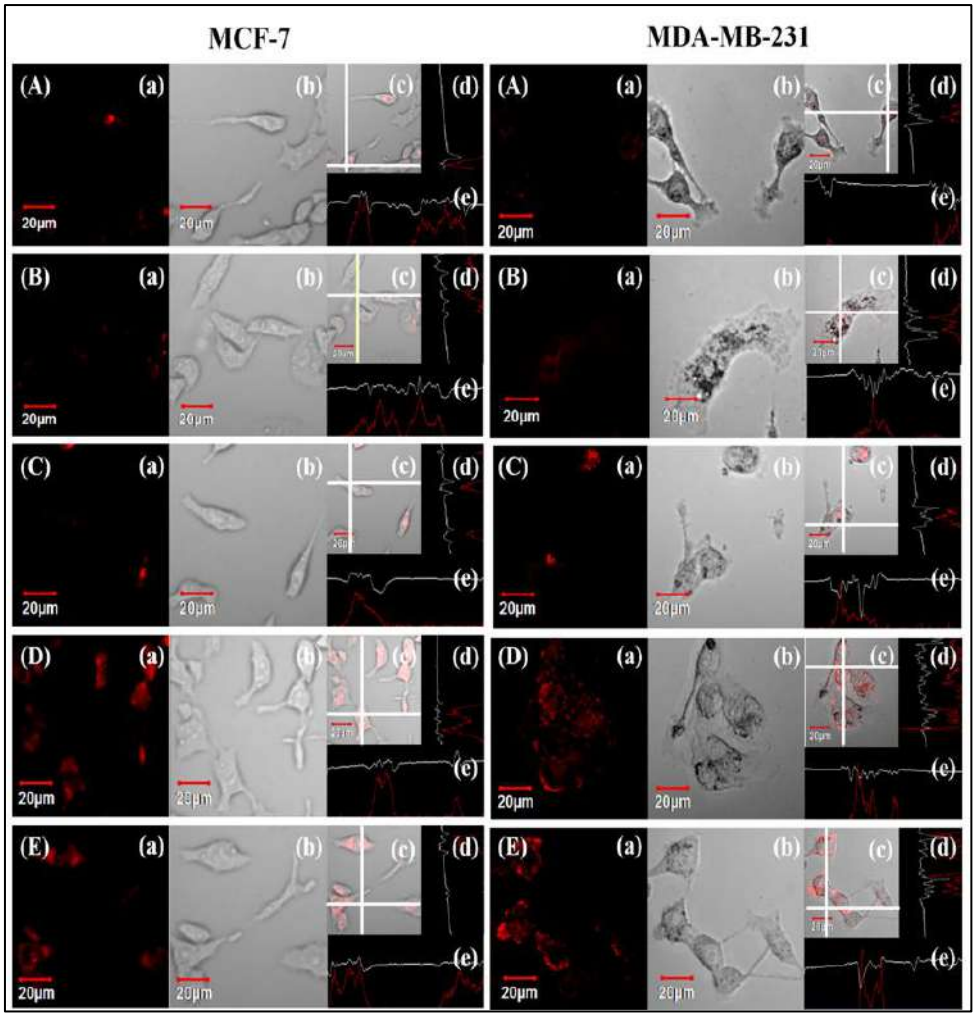

Figure 30: Intracellular fate of (A) DTX, (B) GEM, (C) DTX+GEM (D) DTX loaded BSA NPs (E) DTX loaded AA-GEM-BSA NPs shown by staining with LysoTracker® Red after 24h. Panel (a) Images under the red fluorescence channel of LysoTracker®; Panel (b) Corresponding differential interface contrast images of cells (c) Superimposition of Panel (a) and Panel (b); Panel (d) and (e) in all the images show vertical and horizontal line series analysis of fluorescence along the white line, respectively.

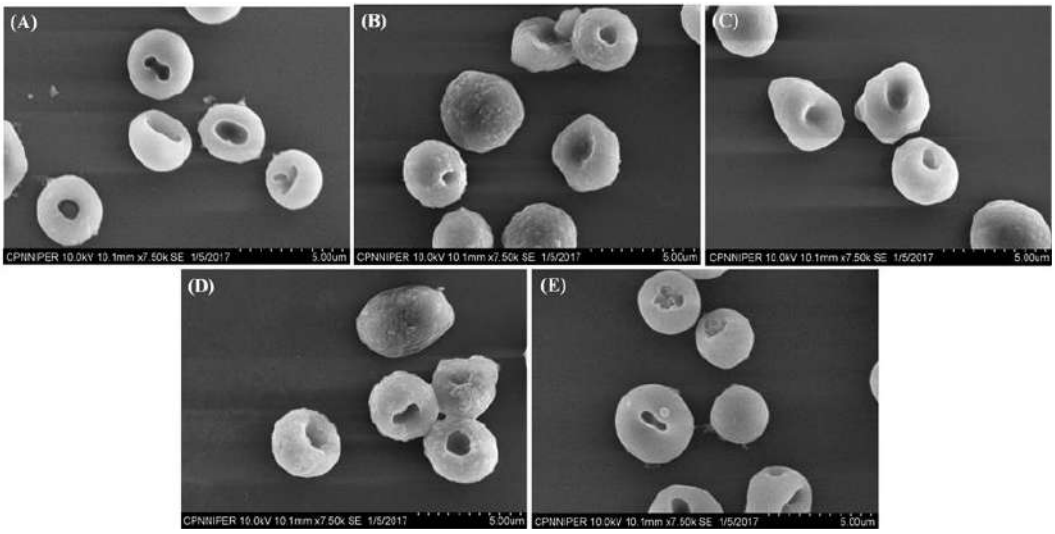

Figure 31: SEM micrographs of RBCs indicative of (A) control and different groups treated with (B) Gemzar®, (C) Taxotere®, (D) Gemzar® + Taxotere®, (E) DTX-AA-GEM-BSA NPs

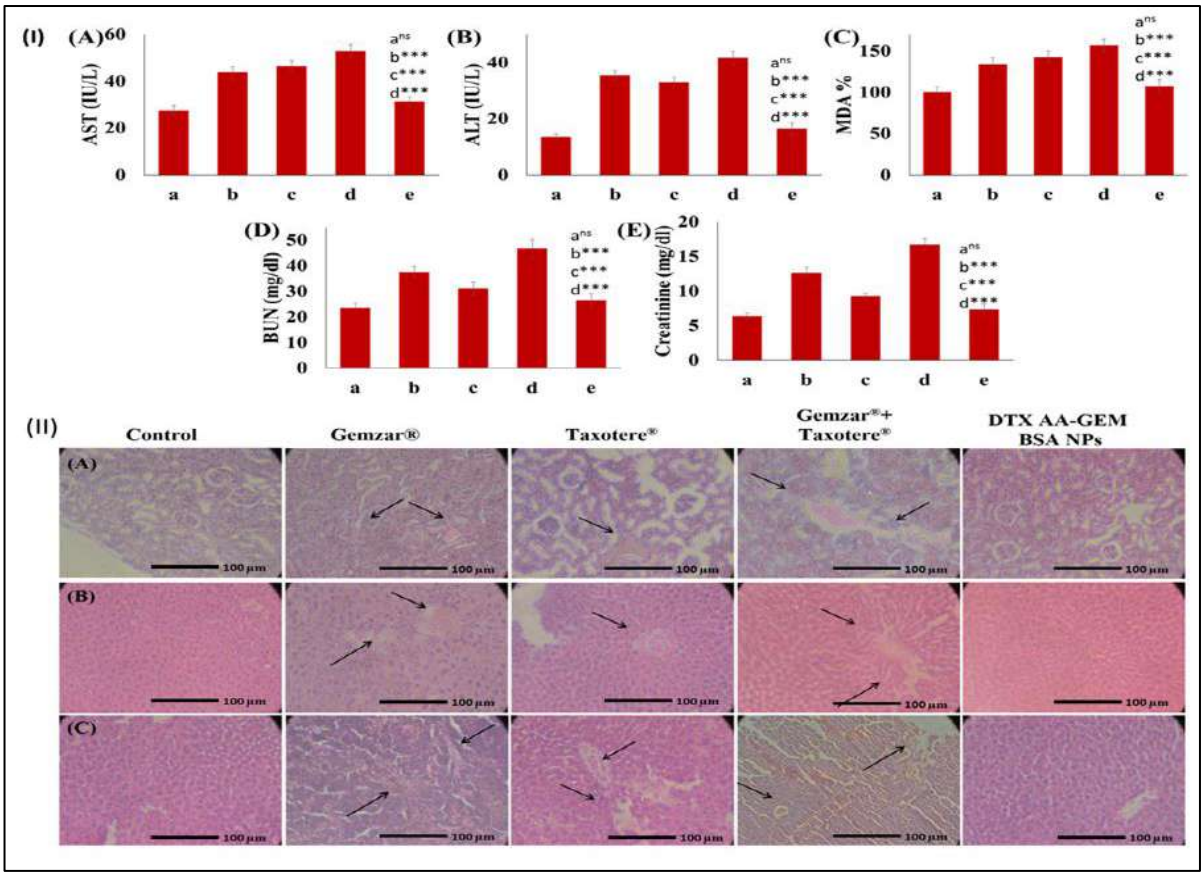

Figure 32: (I) Biochemical markers (A) AST (B) ALT (D) BUN (E) creatinine levels in plasma and (C) MDA level in liver homogenate after 7 days following administration of (b) Gemzar®, (c) Taxotere®, (d) Gemzar® + Taxotere® (e) DTX loaded AA-GEM-BSA NPs as compared to (a) control. Values are expressed as Mean ± SD (n = 5); ***, significant difference at $p < 0.001$, ns, insignificant and (II) Histopathological sections of (A) kidney, (B) liver and (C) spleen following the treatment with free drugs and NPs

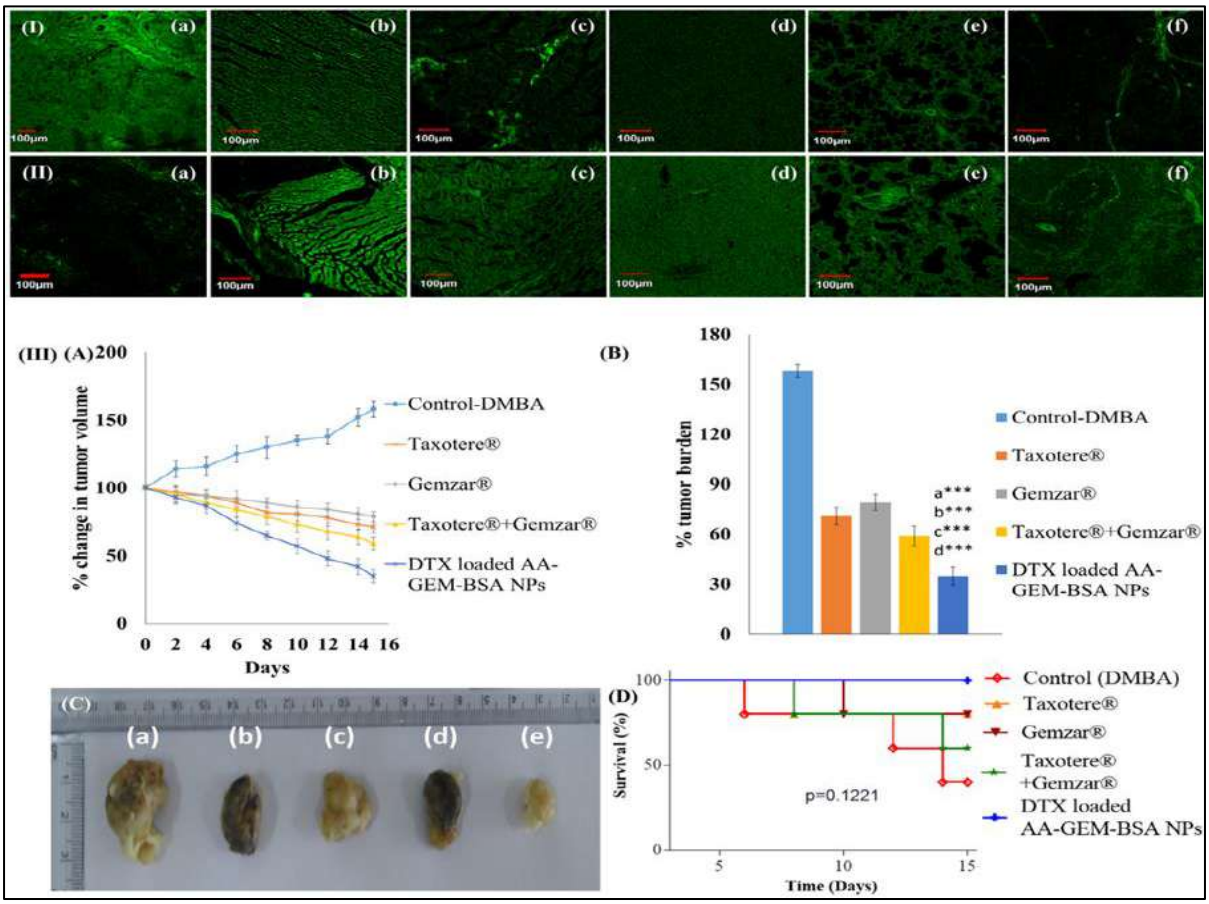

Figure 33: Fluorescence intensity of (I) C-6 loaded AA-GEM-BSA NPs, (II) Free C-6 in (a) tumor, (b) heart, (c) kidney, (d) liver, (e) lung and (f) spleen and (III) (A) Comparison of % change in tumor volume and (B) % tumor burden of different formulations (***, significant difference at $p < 0.001$, ns, insignificant) (C) Representative photographs of excised tumors from different treatment groups and (D) Kaplan–Meier survival curve depicting the survival rate of tumor-bearing animals received different treatments. The P values are for the log-rank test.

Publications:

1. Varun Kushwah, Sameer S. Katiyar, Chander Parkash Dora, Ashish Kumar Agrawal, Dimitrios A. Lamprou, Ramesh C. Gupta, **Sanyog Jain** (2018). Implication of linker length on cell cytotoxicity, pharmacokinetic and toxicity profile of gemcitabine-docetaxel combinatorial dual drug conjugate. **International Journal of Pharmaceutics, 548(1)**, 357–374. (**Impact factor: 5.8**)

2. Varun Kushwah, Sameer S Katiyar, Ashish Kumar Agrawal, Ramesh C Gupta, **Sanyog Jain** (2018). Co-delivery of docetaxel and gemcitabine using PEGylated self-assembled stealth nanoparticles for improved breast cancer therapy. **Nanomedicine: Nanotechnology, Biology, and Medicine, 14 (5),** 1629–1641. **(Impact factor: 5.4)**

3. Varun Kushwah, Sameer S. Katiyar, Chander Parkash Dora, Ashish Kumar agrawal, Dimitrios A. Lamprou, Ramesh C. Gupta, **Sanyog Jain** (2018). Co-delivery of docetaxel and gemcitabine by anacardic acid modified self-assembled albumin nanoparticles for effective breast cancer management **Acta Biomaterialia, 73**, 424–436. (**Impact factor: 9.7**)

- **Brief research report 7**

Macromolecular bipill of gemcitabine and methotrexate facilitates tumor-specific dual drug therapy with higher benefit-to-risk ratio

Combination therapy is a powerful strategy to overcome the limitations of single-drug treatments. It involves using two or more therapeutic molecules together to enhance effectiveness while reducing side effects. However, coordinating the pharmacokinetics and targeting of these drugs is a challenge. Nanocarriers like polymeric nanoparticles and liposomes have been used to deliver multiple drugs to specific sites. While promising, precise control of drug loading and release remains a challenge. One solution is to chemically link multiple drugs with hydrolysable linkers, creating a new drug entity that can address solubility and pharmacokinetic issues. Despite potential benefits, such conjugates are still in early stages of development. There's limited evidence of their effectiveness *in vivo*. We explored the improvement of existing drugs with limited biopharmaceutical properties by synthesizing a novel macromolecular bipill that links methotrexate (MTX) and gemcitabine (GEM) to a heterobifunctional polyethylene glycol (PEG) spacer. These drugs have shown promise in clinical reports but suffer from pharmacokinetic issues. GEM is highly hydrophilic with a short half-life, requiring frequent high-dose administration and leading to toxicity. MTX faces similar challenges. Covalent bioconjugation of GEM and MTX via PEG linker (GEM-PEG-MTX) not only transformed the solubility profiles of constituent drug molecules but significantly improved their stability in presence of plasma. In the *in vitro* cytotoxicity assay, combinatorial conjugates initially showed a slight decrease in cytotoxicity but later exhibited a 1.57-fold increase in potency compared to free drug combinations, attributed to enhanced uptake and improved drug stability. Additionally, In the recovery mode (6-hour exposure followed by 18-hour recovery), GEM-PEG-MTX demonstrated a remarkable 2.09-fold lower IC_{50} value and a significant 2.44-fold increase in the apoptotic index compared to the free drug combination, confirming its enhanced therapeutic potential. The superior anticancer efficacy of GEM-PEG-MTX is attributed to two key factors: Firstly, the enhanced intratumoral localization of the conjugate, facilitated by the stealth PEG linker, capitalizes on the enhanced permeability and retention (EPR) effect. Secondly, this efficacy is further potentiated by the synergistic interaction between the dual pharmacologically active molecules, GEM and MTX, which collectively contribute to the observed enhancement in tumor growth inhibition. The result explicitly supported our hypothesis of synergistic performance of dual drug conjugates over single drug or physical combination of two drugs and reduces their toxicity , higher benefit to risk ratio. Our future studies will concentrate on evaluating the pharmacokinetic profile of GEM-PEG-MTX and correlate the findings with observed synergism.

Highlighted experimental outcomes:

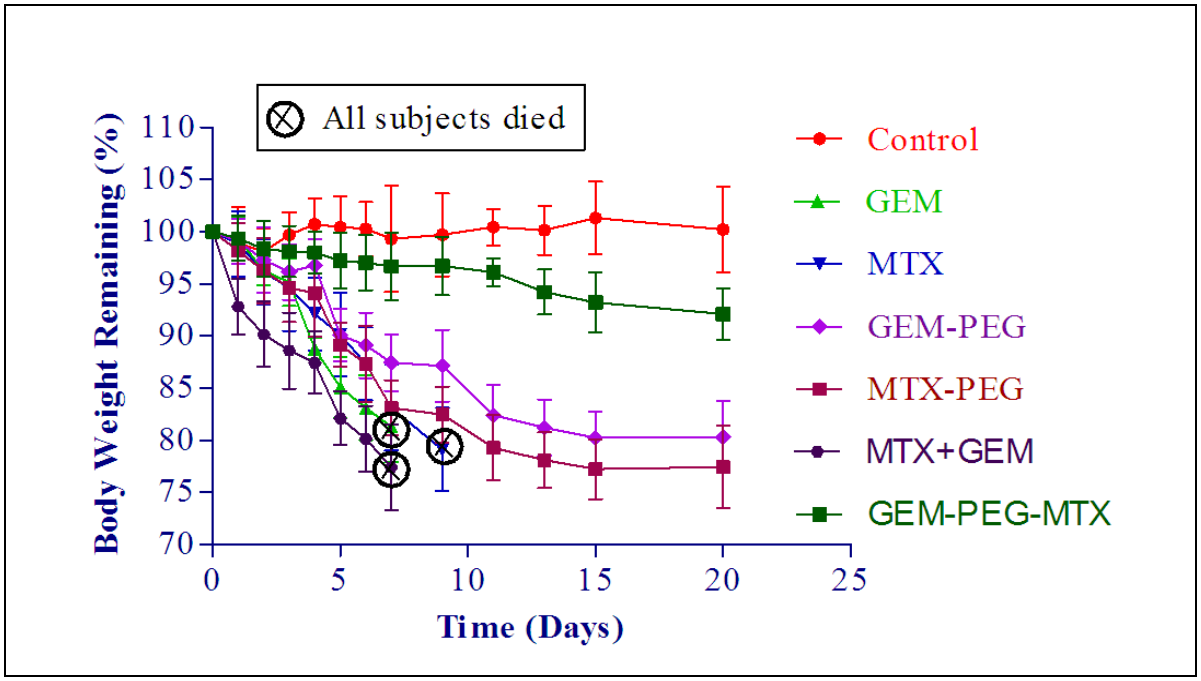

Figure 34: Decrease in body weight following administration of different formulations. Plot indicates the body weight remaining (%) with respect to time.

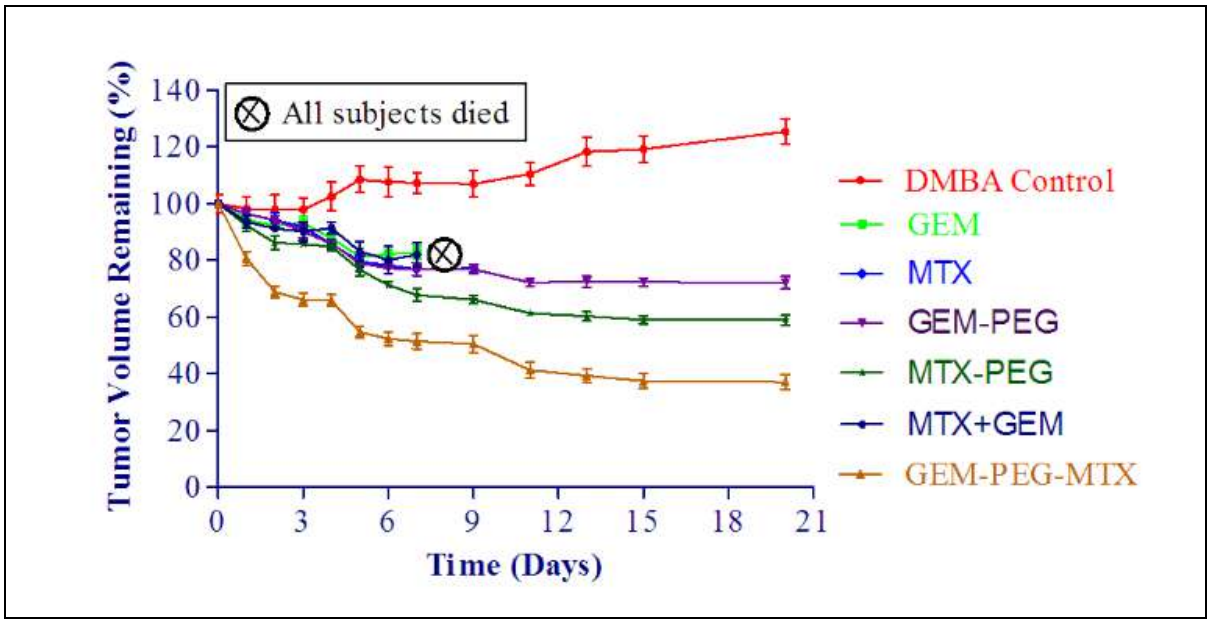

Figure 35: In vivo antitumor efficacy profile of GEM-PEG-MTX bioconjugate, free GEM, free MTX, physical mixture of MTX and GEM, GEM-PEG, and MTX-PEG.

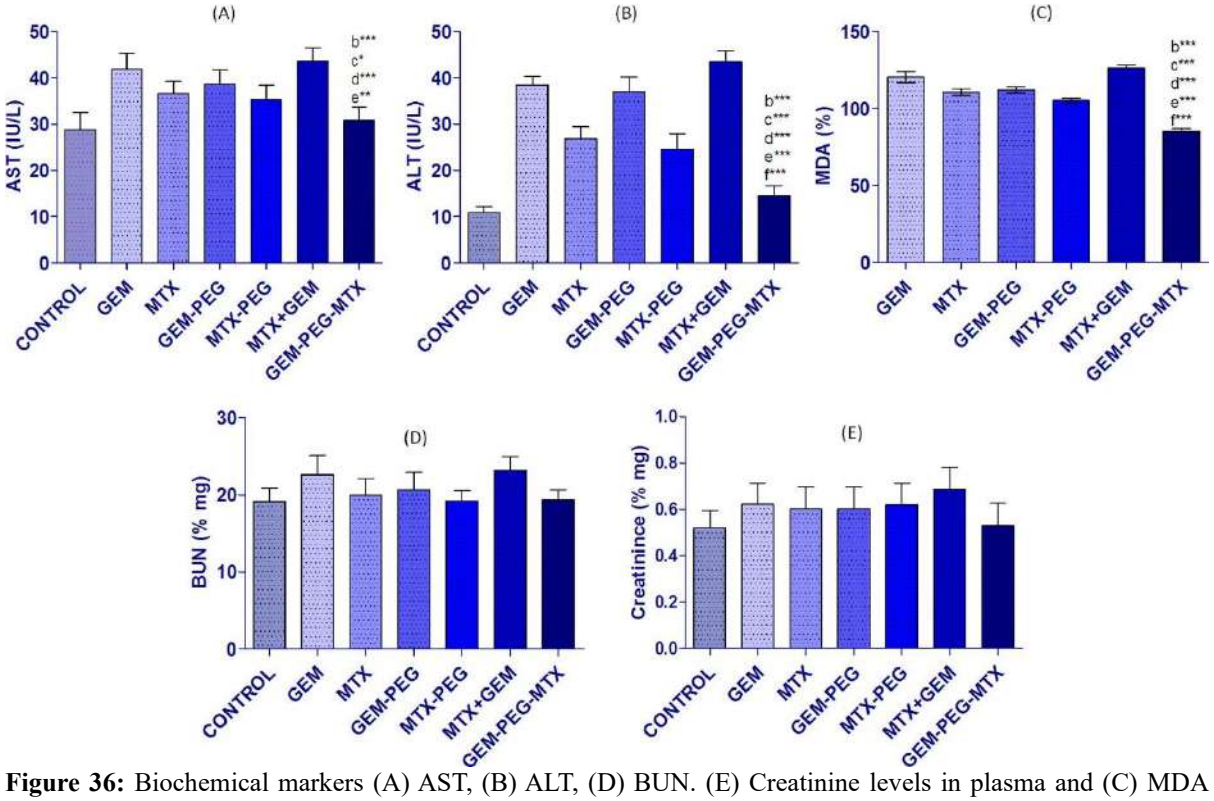

Figure 36: Biochemical markers (A) AST, (B) ALT, (D) BUN. (E) Creatinine levels in plasma and (C) MDA level in liver homogenate following administration of free GEM, free MTX, GEM-PEG, MTX-PEG, physical mixture of MTX and GEM, and GEM-PEG-MTX conjugate

Publication:

Manasmita Das, Roopal Jain, Ashish Kumar Agrawal, Kaushik Thanki**, Sanyog Jain**, Macromolecular bipill of gemcitabine and methotrexate facilitates tumor-specific dual drug therapy with higher benefit-to-risk ratio. **Bioconjug Chem. 2014 Mar 19;25(3):501-9**. **(Impact factor: 4.7)**

- **Brief research report 8**

Bio-conjugation based delivery approach for effective co-delivery of Gemcitabine and Curcumin

In the present work, we have developed a polymeric drug conjugate containing the anticancer drug Gemcitabine (GEM) and the antioxidant Curcumin (CUR). GEM has high hydrophilicity but a short half-life (~45min), while CUR, with both antioxidant and anticancer properties, has low aqueous solubility (~11ng/ml), limiting its clinical application. The conjugate (GEM-PEG-CUR) using a PEG linker addresses solubility and stability issues, balancing hydrophilicity, and hydrophobicity. This approach synergistically enhances anti-tumor efficacy, potentially reducing toxicity as well. The synthesis of the GEM-PEG-CUR conjugate involved three steps: (1) preparing the active NHS ester of CUR, (2) PEGylating the ester with NH2-PEG-COOH, and (3) covalently conjugating GEM. HCl with the activated PEG-derived CUR ester using standard Carbodiimide chemistry. Characterization of both the final conjugate and intermediates was done using UV, FTIR, NMR, and mass

spectroscopy. The melting point of final conjugate was found to be 46℃ which is similar to PEG. Further, GEM-PEG-CUR conjugate showed decreased solubility of GEM (~62 mg/ml) as compared to free drug (~75.05mg/ml) at 25℃. *In vitro* hydrolysis studies demonstrated minimal release of GEM at pH 5.5 which increase at pH 7.4 indicating no influence of enzyme on release of GEM. Similarly, *in vitro* plasma degradation studies showed minimum degradation of GEM with 17% detected dFdU as compared to free drug with 60% dFdU. Furthermore, the cell cytotoxicity potential of the developed bio-conjugates was also noted in recovery experiments which revealed 3.77-fold increase in cell cytotoxicity of GEM–PEG–CUR as compared to that of GEM + CUR. The apoptotic index was found to be remarkably higher in case of GEM–PEG–CUR as compared to that of free drugs alone and in combination. In line with this, conjugate exhibited higher level of 8-OHdG ($p < 0.001$) than free drug in DNA damage assay. Amongst all the treatment groups, animals treated with GEM–PEG–CUR showed significantly higher tumor growth inhibition as compared to those treated with free GEM ($p < 0.001$), free CUR ($p < 0.001$), a combination of CUR and GEM ($p < 0.001$), GEM–PEG ($p < 0.01$) and CUR–PEG ($p < 0.001$). Survival analysis revealed 100 % survival of animals treated with conjugate as compared to free drugs (50% survival).

Highlighted experimental outcomes:

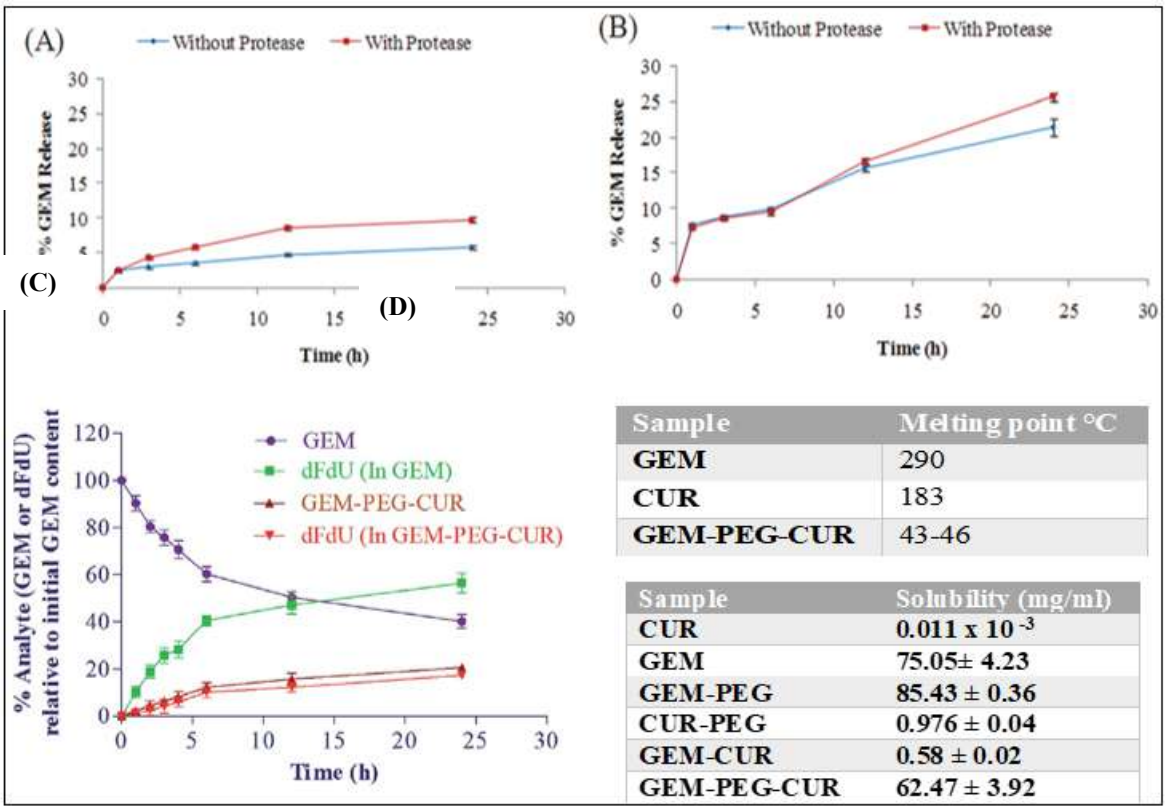

Sample	Melting point °C
GEM	290
CUR	183
GEM-PEG-CUR	43-46

Sample	Solubility (mg/ml)
CUR	0.011×10^{-3}
GEM	75.05± 4.23
GEM-PEG	85.43 ± 0.36
CUR-PEG	0.976 ± 0.04
GEM-CUR	0.58 ± 0.02
GEM-PEG-CUR	62.47 ± 3.92

Figure 37: Represents the *in vitro* stability profile of GEM–PEG–CUR at pH (A) 5.5 and (B) 7.4 (C) Time-dependent estimation of GEM and DFDU in rat plasma (pH7.4) at 37℃. Table highlights the solubility and melting point of developed conjugate and intermediates respectively.

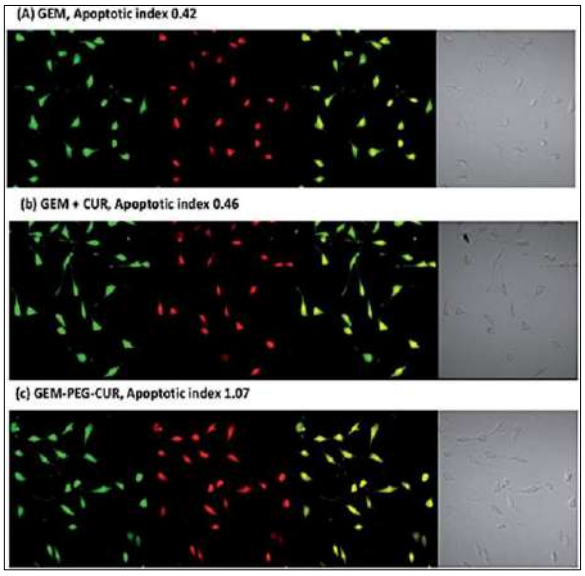

Sample	24h	48h	72h	Recovery mode
GEM	37.12	10.18	5.88	77.18
CUR	24391 4.14	1697.93	235.1 7	>10000 0
GEM-PEG	15.31	9.08	5.39	27.96
CUR-PEG	2354.8 3	1272.61	215.2 0	2828.71
GEM+CUR	31.80	9.23	5.54	73.51
GEM-PEG-CUR	18.50	8.24	5.12	19.45

Figure 38: Apoptosis assay of developed bioconjugate against MCF-7 cells; green channel depicts the fluorescence from carboxy fluorescein (cell viability marker dye); red channel depicts fluorescence from Annexin Cy3.18 conjugate (cell apoptosis marker dye) third channel represents the overlay image whereas fourth window depicts the differential contrast image of representative cells. Table represents IC_{50} values (μM) of GEM-bio-conjugates against MCF-7 cell lines

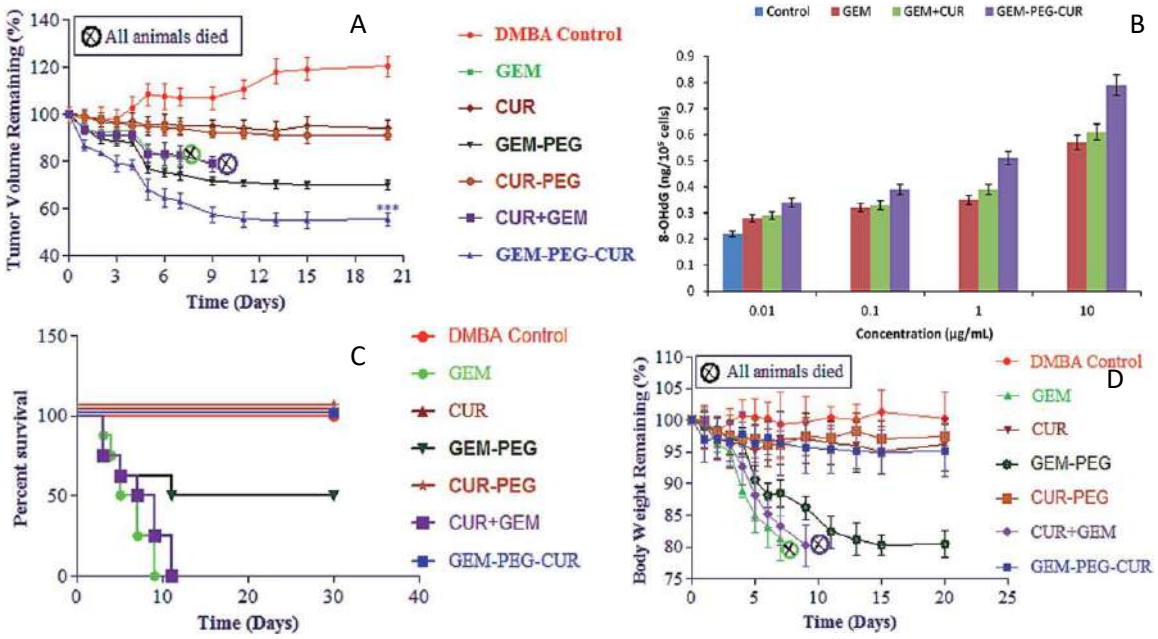

Figure 39: Plot indicates A) The percentage tumor volume remaining with time [a w.r.t control, b w.r.t free GEM, c w.r.t. free CUR and d w.r.t physical mixture of CUR and GEM (CUR + GEM) (***p < 0.001, **p < 0.01) B) 8-OHdG levels in cells treated with GEM and its bio-conjugate in MCF-7 cells C) Kaplan–Meier survival plot for evaluation of animal's survival D) Body weight remaining (%) with respect to time.

Publication:

Sanyog Jain, Roopal Jain, Manasmita Das, Ashish K. Agrawal, Kaushik Thanki, Varun Kushwah, Combinatorial bio-conjugation of gemcitabine and curcumin enables dual drug delivery with synergistic anticancer efficacy and reduced toxicity. **RSC Adv. 4 (2014) 29193–29201. (Impact factor: 3.9)**

प्रो. संयोग जैन / PROF. SANYOG JAIN
फार्मास्युटिक्स विभाग / Dept. of Pharmaceutics
राष्ट्रीय औषधीय शिक्षा एवं अनुसंधान संस्थान
National Institute of Pharmaceutical Education and Research
सेक्टर - 67, एस. ए. एस. नगर - 160 062, पंजाब, भारत
Sector-67, S.A.S. Nagar-160 062, Punjab, INDIA

Date: August 28, 2023